GEOMAGNETIC STORM AND ITS IMPACT ON TIME-DEPENDENT TRANSFORMER THERMAL RESPONSE IN LARGE POWER SYSTEMS

A Thesis

by

RIDA FATIMA

Submitted to the Graduate and Professional School of
Texas A&M University
in partial fulfillment of the requirements for the degree of

MASTER OF SCIENCE

Chair of Committee,	Adam B. Birchfield
Committee Members,	Thomas J. Overbye
	Jeyavijayan Rajendran
	Jennifer Marshall
Head of Department,	Costas Georghiades

August 2023

Major Subject: Electrical Engineering

ABSTRACT

Geomagnetically induced currents (GICs) in power systems are a potential source of introducing DC in transformers, resulting in undesirable occurrences of additional harmonics and higher temperatures. The purpose of this thesis is to analyze the behavior of transformers in a large-scale power system under the influence of GMD. Looking at the bigger picture, the idea is to model the risk on a synthetic grid in order to improve the system's resilience. By modeling severe GMD events from various derivations of NERC Benchmark Event, it gives us a visualization of how big of a GMD event is needed to be concerned about the stability of the power system.

This thesis reviews the methodology and results of the case studies that were performed on the transformer fleet of a 2000-bus synthetic grid on the geographic footprint of Texas. The thermal assessment technique identifies the transformers with potential thermal impacts using a first-order hotspot calculation method for the structural parts of the power transformer. Firstly, a thermal model for approximating the hotspot temperature rise is developed. The total hotspot temperature obtained from the thermal model is used to determine the transformers that violate the condition-based GIC susceptibility categories depending on how long the transformers have been in service. The analysis is undertaken by modeling severe GMD events—NERC benchmark event and its derivatives—to assess how the transient hotspot behavior of a power transformer is related to various environmental conditions, such as electric field magnitude and direction, transformer neutral current, and storm duration.

This thesis also aims to present a methodology for creating severe synthetic GMD storms with the primary goal of testing the resiliency of the power system. To accomplish this, the time-series fragments of Electric field data extracted at random from the NERC benchmark event undergo spatial and temporal transformation. The resultant 'modified' fragments are concatenated to form a synthetic temporal E-field dataset. Many iterations of this process can result in a range of synthetic storms that vary in duration, intensity, and direction. The extremity of a synthetic GMD storm is then investigated through the lens of transformer thermal assessment on the 2000-bus synthetic

case. This can aid in gaining heightened system awareness in the possible event of an extreme GMD event.

In conclusion, this thesis can facilitate in narrowing the focus to the susceptible components of the bulk-power system during an extreme GMD event so that GIC mitigation strategies could be devised accordingly to maintain a resilient power grid.

ACKNOWLEDGMENTS

The research journey had its fair share of ups and downs; there were days when stars were aligned and research seemed to progress, but there were also days when it seemed like there was no light at the end of the tunnel. Having an adviser, who was also a great mentor, helped me turn my self-doubt into belief. He was the guiding light of my research. I am extremely grateful to my adviser, Prof. Adam Birchfield, for his wisdom, vision, and guidance which were integral to the progress of this work.

I am grateful for the family-like friends I found at Texas A&M University. Sanjana, a sister in a foreign land, your words of motivation made every impossible possible for me. Oluwatoyin, your infectious laugh always gave me joy and your positivity kept me going even when I was shrouded in doubt. To the whole power engineering group, I got to learn so much from you. Thanks for cultivating a welcoming and fun learning experience, it made my graduate school experience so much more memorable and enjoyable.

I am forever indebted to my parents, Hassan and Saleha, for their unwavering support and unconditional love. You have always been my anchor, and this was no exception. Thank you for the check-in phone calls every single day that made everything instantly better. Thank you to my younger siblings— Salima, Mehak, Shahbaz and Wardah— for being my best friends for life, for always cheering for me, and for being my forever support system.

I would like to thank my grandparents. Especially my grandfather in heaven, whom I lost recently. Thank you for reminding me to show grace to everyone, for being a big advocate for education, for the invaluable life lessons, and for our hour-long conversations.

Finally, my husband, Zain. You were always there, whenever and wherever that was. Thank you for listening to me rant, for proofreading, for giving me reasons to laugh when things became too serious, for unwavering patience and support, and for consistent reminders of motivation.

Most of all, I am thankful to God for being so kind to me, for listening to my countless prayers, and for blessing me with great opportunities, family, friends, and professors.

CONTRIBUTORS AND FUNDING SOURCES

Contributors

This work was supported by a thesis committee consisting of advisor Prof. Adam B. Birchfield, Prof. Thomas J. Overbye, and Prof. Jeyavijayan Rajendran, of the Department of Electrical and Computer Engineering, and Prof. Jennifer Marshall of the Department of Physics and Astronomy. All work conducted for the thesis was completed by the student independently.

Funding Sources

The work was funded in part by the Thomas W. Powell '62 and Powell Industries Inc. Fellowship from the Department of Electrical and Computer Engineering at Texas A&M University.

The work was funded in part by ERCOT's Joe Weatherly Memorial Scholarship.

TABLE OF CONTENTS

Page

LIST OF FIGURES

FIGURE Page

LIST OF TABLES

TABLE Page

1. INTRODUCTION

1.1 Background

In the quest for maintaining the reliability of the electrical power systems under all circumstances, it is significant to study the factors that can make the electric grid vulnerable to major disturbances. One such disturbances is sourced by Sun's solar activity. These solar flares ejected from the sun are often termed as 'Geomagnetic storms" which have the potential to distort Earth's magnetic field, thereby resulting in Geomagnetically Induced Currents (GICs) in conductors such as transmission lines that are connected via grounded neutrals of wye-connected transformers.

On March 13, 1989, a K-9 geomagnetic storm — a geomagnetic storm with the highest K-Index — struck the Hydro Quebec system, plunging most of the province of more than 6 million residents into darkness for almost 9 hours. The half-cycle saturation of the power transformers due to GICs are the root-cause of many problems in bulk power system; the consequences include additional harmonics, increased reactive power demand, and internal localized heating of the transformers [9], [10]. On that day, a combination of these impacts due to half-cycle saturation resulted in a blackout of the Quebec power grid. The excessive harmonics took seven static-VAR compensators off-line, leaving a void in voltage regulation. That loss, aggregated with the increased consumption of reactive power due to transformers operating under half-cycle saturation, posed dire problems of voltage regulation. About 8 seconds after SVCs were shutdown, a 735 kV transmission line tripped and the propagation of transients had a cascading effect on tripping other 735 kV transmissions on La Grande network.

While the Quebec grid experienced blackout, the Eastern United States also suffered from the havoc effects of the March 13 episode. Particularly at Salem Nuclear Plant in NJ, the excessive heat produced by half-cycle saturation of the generator step-up (GSU) transformer severely damaged the equipment. The replacement of this transformer yielded a cost of several million dollars [11]. In the interim, the generation from the Salem plant was interrupted. These large-scale outages,

such as the example listed previously, have significant economical impacts from loss of revenues because of the interrupted electricity generation to the replacement costs for thermally damaged transformers.

Predicting the development of solar storms is laced with uncertainty due to a lack of data points for extreme GMD events. While the next occurrence of a strong GMD is difficult to predict, one thing is certain that, GMD will continue to affect the operation and reliability of the modern power grid, more so now, as the transmission systems have become more interconnected spanning over large geographical areas and even more complex. Even though the direct impacts of GMD on transmission lines are mainly reported, the distribution system can be indirectly affected as well. In the event of post-transformer failure, constrained areas in terms of power supply can arise. Since large geographic areas are exposed to GICs, the existence of redundancies in the transmission grid might not always help mitigate the risk of blackouts [12].

1.2 Problem Statement

Power transformers are salient elements in the transmission and distribution of electrical energy, therefore, it's of prime importance to minimize the risk of transformer failure due to overheating during a GMD event to ensure reliability of the grid. A power transformer is designed, such that, under normal conditions, it operates in the linear range of the B-H curve — right below the knee region of the magnetizing curve. This way, a small exciting current is required to provide the magnetic flux needed for the transformation of voltage.

With an addition of dc source to the transformer, it generates a dc-offset on the ac currents. Similarly, when GICs — which are characterized by low-frequency quasi-DC currents — are injected into power transformers, the transformer's core experiences saturation over a portion of the half cycle. With a dc superimposed on ac, a portion of this process is pushed into the non-linear saturation region of the B-H curve, where additional ampere-turns would produce the same amount of flux. This non-linear behavior of the transformer core is shown by the magnetic flux density vs. current(B-I) graph represented by Fig. 1.1. Therefore, this half-cycle saturation requires a higher magnitude of non-symmetric magnetizing current and results in non-linear current rich in even and

odd harmonics.

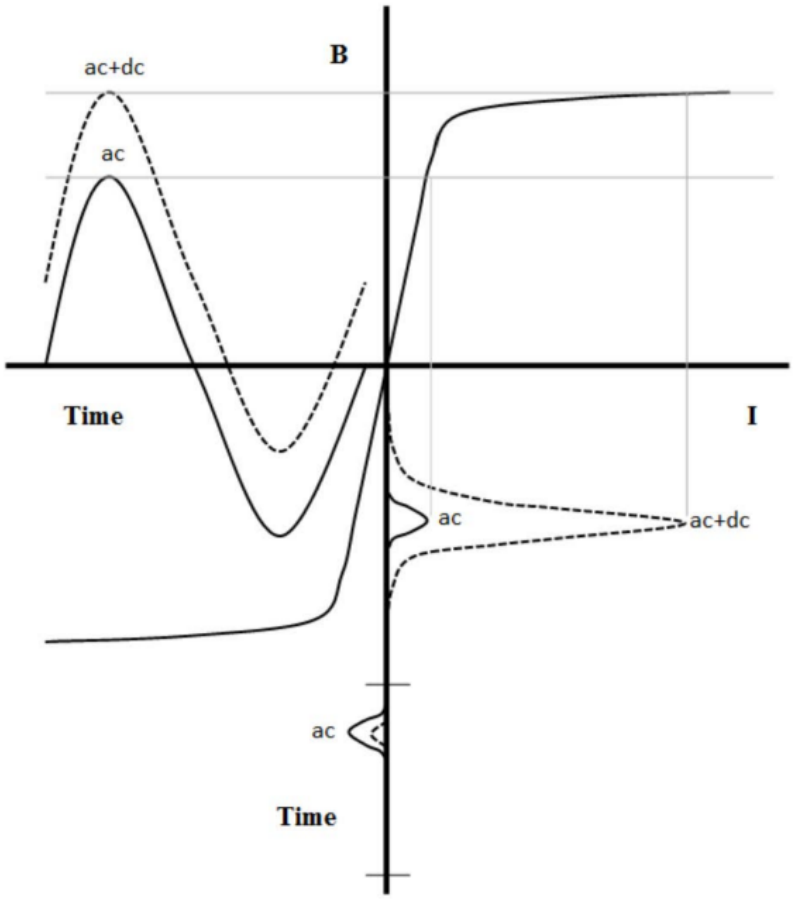

Figure 1.1: Half-cycle saturation caused by quasi-dc GICs [1]

Two of the profound effects of half-cycle saturation are the generation of harmonics and localized transformer heating. The rich-in-harmonics magnetizing current increases the amount of reactive power absorbed by the transformer, disturbs the operation of protective relays, overloads the capacitors, and can potentially cause a system collapse. With the transformer core saturated, it offers a higher reluctance path. As a result, the stray flux escapes out of the core and penetrates other structural members such as windings, tank plates, and clamping structures. Stray flux heating could give rise to local hot spots.

The replacement of high voltage bulk transformers, including generator step-up and step-down transformers, is costly and time-consuming [13]. It's hard to measure the hot-spot temperature of the localized segment, be it the winding or structural part of the transformers; therefore, it is imperative to develop a thermal model that can assess the hot-spot temperature of the transformer and analyze the ones vulnerable to GMD event. This information regarding the at-risk transformers can aid in power system planning and asset management.

This thesis focuses on developing a reasonable understanding of the transformer thermal model for heightened system awareness in the possible event of a GMD storm. The existing 2000 bus synthetic electric grid model is utilized to gain system knowledge and determine the most vulnerable transformers, thereby, redirecting user's attention towards susceptible fractions of the grid which consequently improves the efficiency of the analysis. Throughout this work, I chose to study the effects of GMD on the electric grid using NERC (North American Electric Reliability Corporation) benchmark events, as it has been dealt with in research works in the past [14]; this simulates the worst-case scenario of GMD event which may be applicable to set the threshold limits on the power grid and identifying the transformers on the brink of the vulnerability [15]. Alongside examining the impact of 1989 NERC Benchmark Event on the Texas synthetic grid, I have also derived multiple scaled events in order to investigate the consequences of environmental factors on the possible thermal damage of transformers. Adopting the benchmark event and its derivatives, as prototypical extreme event scenarios could also be useful for emergency preparedness purposes. In this research, an automated transformer thermal tool is developed, by approximating the Laplace domain solution using trapezoidal numerical method.

1.3 Thesis Outline

1.3.1 Introduction

The first chapter provides some background information about the source of the GICs, the interconnection of GICs to the Bulk Power System (BPS), and the negative consequences of GICs in the power grids. The behavior of transformers in the presence of GICs is demonstrated in detail.

Based on these repercussions, the importance of risk assessment of transformers in light of the transformer thermal model is highlighted.

1.3.2 Literature Review

The second chapter details the highlights of extreme GMD scenarios from a historical lens. This section also describes the methodology of how the electric field is induced in the transmission lines and how the GICs induced by the electric field are calculated for power system modeling, which is then used to evaluate the susceptibility of the power transformer to GICs.

1.3.3 Hotspot Calculation

This chapter of the thesis develops a thermal model approximation for structural components of the transformers(i.e. tie-bars) in order to evaluate the hotspot temperature rise in transformers for under the influence of GICs. The thermal models are validated against the thermal response results from [5].

1.3.4 Case Studies on Transformer Thermal Assessment

Using the NERC benchmark event to develop the GIC model on a large-scale 2000-bus synthetic grid, the thermal response of a transformer fleet consisting of 861 transformers is analyzed. This chapter presents the case study results of transient hotspot behavior under various environmental factors such as electric field magnitude, direction, and storm duration.

1.3.5 Creation and Application of Synthetic GMD Storms on Transformer Thermal Assessment

In order to close the research gap where researchers lack an extensive range of extreme GMD scenarios due to their low-frequency occurrence, this section presents a framework for creating extreme synthetic GMD storms. The thermal assessments of transformers with respect to a set of 100-generated synthetic storms are summarized.

1.3.6 Summary and Future Work

To conclude the thesis, the case study results of transformer thermal assessments from the large-scale synthetic grid are summarized. This research opens avenues for further related research work that can improve the resilience of power grids in the wake of unprecedented geomagnetic disturbances.

2. LITERATURE REVIEW

2.1 A Spotlight on GICs

Threats to power system reliability were unfolded during the rarely occurring extreme geomagnetic storm of March 13th, 1989, moving at a peak variation of 500 nT/min—a rate of change in geomagnetic field. The induced GICs hampered the operation of Hydro-Quebec power grid, causing a blackout of the grid in less than 2 minutes [16]. The outage lasted for about 9 hours and affected millions of people. Hydro-Quebec's neighboring systems in the United States, particularly, New Jersey came close to experiencing the unpleasant consequences of voltage collapse along with the thermal failure of a generator step-up transformer at Salem Nuclear Plant [17]. In another GMD event of 1992, a well-monitored 300 MVA transformer captured a temperature rise from 60 degrees C to over 175 degrees in just as little as 10 minutes [18]. Considering the onset of an extreme GMD event, the thermal damage can be compounded by repeated exposure to GICs and a longer duration of an extreme geomagnetic storm which can typically last for days. The storm of March 1989, hailed as the largest geomagnetic storm of the last century, had the most catastrophic impacts on the grid [11]; however, it doesn't secure the title of the strongest storm to be ever recorded in the history. Carrington Event of September 1859 is estimated to be the most severe solar storm that reached approximately -2000 nT/min [19]— almost 4 times more than March 13th, 1989's event. As a result, some telegraph systems in North America and Europe were destroyed [20]. In 1859, the electric infrastructure was not in place, not until 1882; therefore, the impact of GMD in September 1859 wasn't as plausible as of March 1989, a time when much of the civilization was already dependent on the working power grid. The economic impact was estimated to be C$ 13.2 billion [21]. With the magnetic fluctuations being four times or more than the March 1989 storm, one can imagine how catastrophic the footprint of an extreme storm can be on the grid.

The sun follows a solar cycle of approximately 11 years. To study the behavior of the sun,

observers have tracked sun spots: the regions on sun with high magnetic field and low temperature as compared to the surrounding areas. In the timespan of almost 11 years, the amount of sun spots varies from solar minimum to solar maximum. Currently, the sun is underway its 25th solar cycle, with a peak expected in 2025. During a solar maximum, the solar activity which includes solar flares and coronal mass ejections (CMEs) grows larger. The geomagnetic activity cycle peak produced by the sunspot cycle's peak usually lags by 3-5 years. Even though the probability of the occurrence of geomagnetic storm during the peak of solar activity is high, it doesn't eliminate the chance of severe GMDs happening during off-peak solar cycle like the March 13, 1989 storm [7]. This introduces increased uncertainties in accurately predicting the next extreme GMD event.

In fact, the sprawling expansion of the HV transmission grid over the past few decades [22] which spans across large geographic distances almost acts like a grounded antenna to the induced electric field by GMD event, thus increasing the space weather vulnerabilities even more. Moreover, GIC effects have also been documented at mid- and low-latitude locations [23][24], proving that extreme GMD scenarios are no longer a high-latitude phenomenon but rather a global one.

2.2 Space Weather Indices for Measuring GMD

The National Oceanic and Atmospheric Administration (NOAA) monitors the intensity of the geomagnetic storms using Planetary K-index. The Kp index based over a 3-hour interval of maximum magnetic fluctuation (measured in nT) was first introduced by J. Bartels in 1949. Most of the power utilities have employed K-indices to characterize the magnitude of GMD-event [7] on a quasi-logarithmic scale of 0-9; 0 being quiet conditions with low magnetic activity and 9 being the most severe geomagnetic activity. The Planetary Kp index is derived by finding the mean of k-index from 13 magnetometer observatories located globally at various geographical locations at different latitudes and longitudes [6]. Geomagnetic storms with K-index more than 5 can disrupt the magnetic field of Earth enough to have noticeable impact on power grid [7], for example, the GMD event of March 13, 1989 was indexed at K=9.

The following Table 2.1 is displaying the K-index and its respective magnetic fluctuations for different categories of the storm.

Table 2.1: K-index in co-relation with the intensity of geomagnetic storms [6], [7]

K-index	**Magnetic Fluctuations(nT)**	**Geomagnetic Activity Category**
0	0-5	Quiet
1	5-10	
2	10-20	
3	20-40	Unsettled
4	40-70	Active
5	70-120	Minor Storm
6	120-200	Major Storm
7	200-330	Severe Storm
8	330-500	
9	>500	

The K-index, however, doesn't account for the rate of change of magnetic variation due to solar activity; for this reason, K-index is not an accurate indicator of a GMD event since earth conductivity models and the rate of change of magnetic field are important factors in determining the effects of geomagnetic storm, as discussed in the following subsection.

2.3 Calculation of Geoelectric Field

Temporal geoelectric field calculation from a real GMD-event is important to determine time-series GIC flow, which in turn can help in the thermal analysis of transformers. The magnetometer or magnetic observatory measures time-series Earth's magnetic field. These measurements can be used to determine the induced geo-electric field. Since the induced GICs are quasi-dc in nature with an associated frequency of 0.00001 Hz to 1 Hz, variations in the magnetic field can penetrate the Earth by hundreds of kilometers. So, it's imperative to adopt a laterally uniform 1-D layered earth conductivity model to look at the conductivity values in the different layers of the Earth all the way down to the mantle as the one shown in Fig. 2.1.

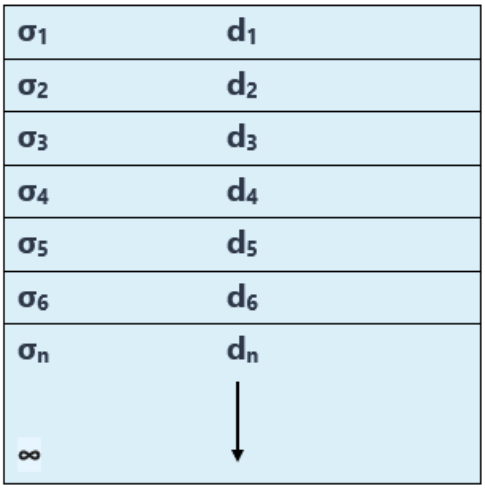

Figure 2.1: 1-D layered Earth conductivity model, adapted from [2]

In order to calculate the electric field spectral value, E(ω), frequency domain techniques such as Fast Fourier Transform (FFT) is employed to calculate the frequency-dependent response of earth at each frequency component of the magnetic field. The calculation of the surface impedance, Z(ω), for each frequency depends on the topological characteristics of the magnetometer's location. This process requires a recursive process of taking the angular frequency, conductivity and thickness of the layer, propagation constant, and reflection coefficient for each layer starting from the bottom layer all the way through the top surface of the earth. Finally, the frequency components along with the respective surface impedance can be summed up to give the electric field spectral value, E(ω), as shown in the equations below.

$$E_x(\omega) = -Z(\omega)B_y(\omega)/\mu_0 \tag{2.1}$$

$$E_y(\omega) = Z(\omega)B_x(\omega)/\mu_0 \tag{2.2}$$

where $E_x(\omega)$ is the Northward electric field(V/km), $E_y(\omega)$ is the Eastward electric field(V/km), $Z(\omega)$ is the earth's surface impedance, $B_x(\omega)$ is the Northward Magnetic field), $B_y(\omega)$ is the Eastward Magnetic field, and μ_0 is the magnetic permeability of free space. The Electric field in

the time domain is calculated by taking the inverse Fast Fourier Transform of the spectral electric field values.

2.4 Scaling of Geoelectric Field

Local earth conductivity along with the geomagnetic latitude can affect GMD storm's intensity. When using the reference geoelectric field time series but for a different geophysical region, the electric field should be scaled according to the conductivity scaling factor of that region. Regions with high earth conductivity result in low scaling β factors and vice versa. Since the benchmark GMD event corresponds to geomagnetic latitude of 60 degrees, it should be scaled with respect to different regions, as described in the in [25]. This captures that electric field intensity decreases with geomagnetic latitude.

$$E_{peak} = E_{max} \times \alpha \times \beta \tag{2.3}$$

where E_{max} is 8 V/km, α is geomagnitude scalar and β is earth conductivity scalar and E_{peak} is the regional electric field peak amplitude.

2.5 Power System Modeling for Calculating GIC

In order to assess the GICs flowing in the power system, it's important to compute the geoelectric field from the geomagnetic data collected from magnetometer and the earth conductivity model for that respective region [2]. Due to the geoelectric field, the earth surface potential is induced on transmission lines connected between two grounded neutrals of Y-connected transformers, as shown by Fig. 2.2. Therefore, the geoelectric field is then used to calculate the dc line voltage, V_{dc}, by integrating the electric field over the incremental length of the transmission line, assuming a uniform electric field. The resulting V_{dc} is inserted as a dc voltage source in series with the line's resistance. It can be noted that GMD-induced voltage is directly proportional to the length of transmission line, as shown in the equation below:

$$V = E_N L_N + E_E L_E \tag{2.4}$$

Where E_N and L_N are the Northward Electric Field(V/km) at the location of transmission line and Northward length(km)of the transmission line between two grounded Y-connected transformers respectively, and E_E and L_E are the Eastward Electric field(V/km) at the location of transmission line and eastward length(km) of transmission line between two grounded Y-connected transformers, respectively [26].

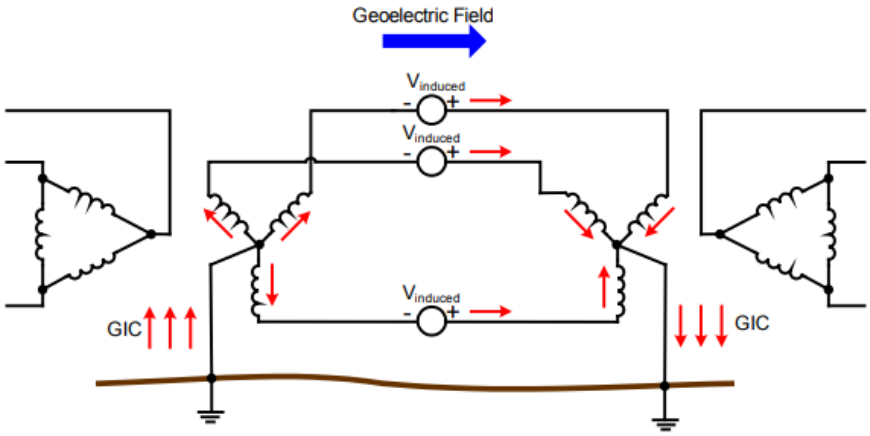

Figure 2.2: Voltage induced by geoelectric field drives GICs to/from grounded transformer neutrals into transmission line [1]

$$I_{dc} = \mathbf{GV} \tag{2.5}$$

The GIC flows in the electric transmission lines are determined by employing dc circuit analysis techniques, due to their inherent quasi-dc characteristics. The aforementioned factors such as the electrical resistance of the substation, length of transmission lines, and type of transformers can affect the level of GICs induced. Therefore, the resistance of the transmission line, transformer winding resistance, and substation grounding resistance is accounted for in the square matrix **G**. While **V** is a voltage vector containing values for dc voltage at substation neutral and bus.

Transformers are conventionally represented in per phase current or effective GICs/phase notation. With the assumption of having a balanced 3-phase system, calculating a single-phase current

for transformer, $I_{per-phase}$, is straightforward which can be found by [26].

$$I_{per-phase} = \frac{I_{GIC,3\phi}}{3} \tag{2.6}$$

The value of effective per phase current is dependent upon the transformer's type; a grounded wye-delta transformer's effective per phase current would be the current at high voltage grounded winding, while an autotransformer's effective per phase current is the sum of currents into both of the windings.

2.6 Evaluating Power Transformer's Susceptibility to GICs

Assessing the susceptibility of transformers to GIC flows requires considering the location of transformer, and the resistance of the soil which in turn determines the level of GICs transformers would be exposed to. Secondly, literature has established that a transformer's sensitivity to DC is influenced by its design parameters including core type, type of transformer (Generator Step-up vs. autotransformer), number of DC-carrying turns on the windings, and voltage rating [3]. For example, single-phase power transformers are statistically proven to be more susceptible to GICs than three-phase transformers, while three-leg core type transformers are the least susceptible [27]. This is because the three-phase, three-limb core-form transformer offers a high reluctance path from the core top yoke all the way through the tank bottom [3]. Fig. 2.3 demonstrates the impacts of DC's flux path according to different core types of transformers. By combining both design-based susceptibility and GIC-level-based susceptibility, the total susceptibility of transformers facing the GIC event can be determined. Another measure of transformer thermal assessment is by considering not only the peak magnitude but also the time duration of the GIC. When transformers are repeatedly exposed to high magnitudes of GIC, the cumulative damage can place transformers at risk of failure [7].

The following sequence places the design-based transformers according to the sensitivity to GIC flow in an ascending manner (from low to high):

1. Three-phase, core-form, three-wound limbs transformer

2. Three-phase, core-form five-limb transformer (three-wound limbs and two flux-return limbs)

3. Three-phase shell form seven-limb core transformer

4. Three-phase shell form conventional core

5. Single-phase core or shell form

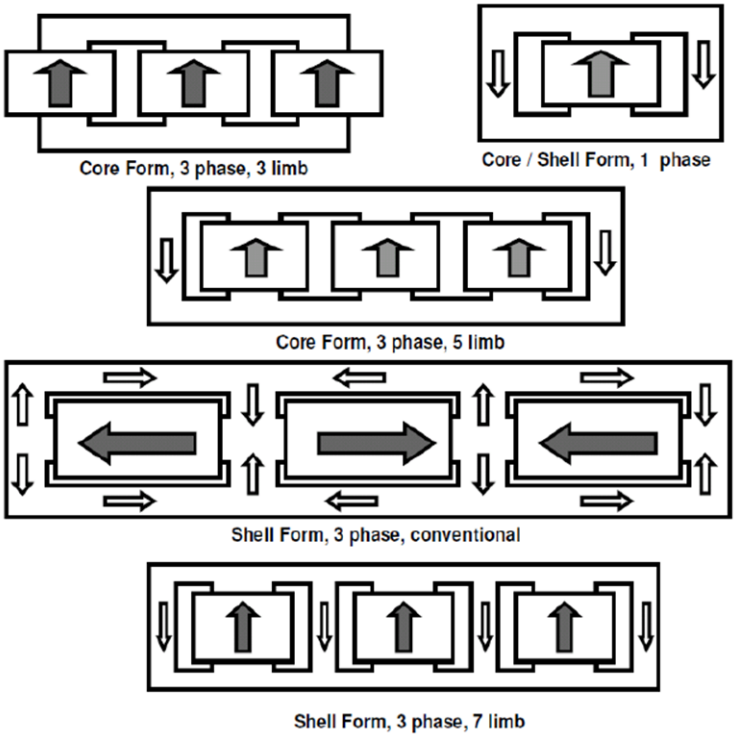

Figure 2.3: Core types and its DC's flux path [3]

3. HOTSPOT CALCULATION

3.1 Transformer Thermal Model

The thermal response of transformers depends on GIC's signature: the time period of the event as well as the magnitude of currents. Fig. 3.1 reflects the transient nature of the GICs with a series of short DC pulses of varying magnitude rather than a constant DC level for a duration of time. In this scenario, it is essential to not only focus on the steady-state behavior of the transformer but to examine temporal transformer behavior during the entirety of the GIC profile, for a correct determination of the hotspot heating.

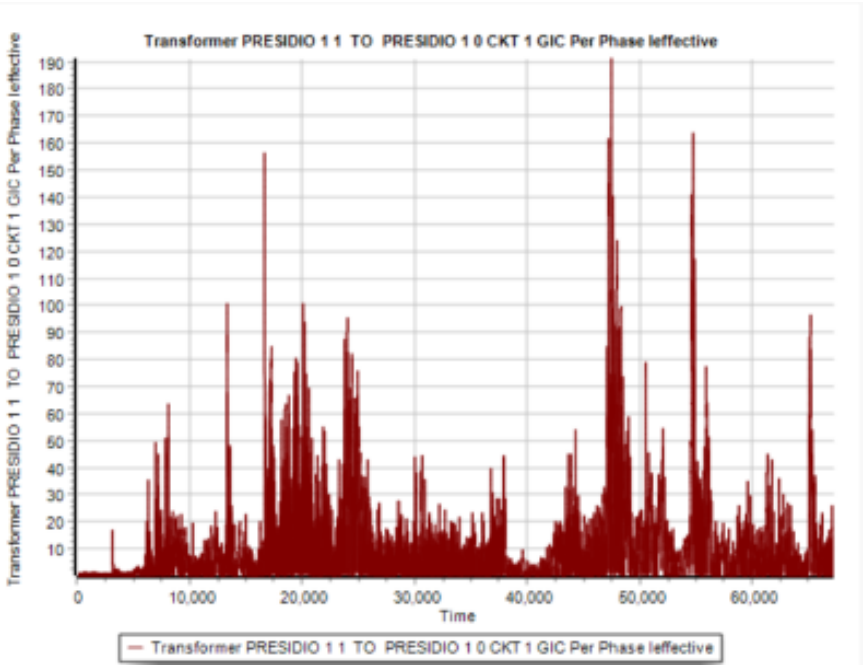

Figure 3.1: Simulated GIC profile in a transformer neutral on 2000-bus synthetic grid

For a constant DC injection, transformer thermal response can be estimated via results from test measurement data or generic published values. Fig. 3.2 shows that the hotspot temperature rise, for a constant dc current injection of 16.67 A/phase in a 400 kV power transformer, increases

exponentially until it nears the steady-state hotspot rise corresponding to that particular DC level. This exponential rise can be characterized mathematically by the Eq. 3.1.

$$\Delta\theta_{hotspot} = \Delta\theta_{ss}(1 - e^{-\frac{t}{\tau}}) \tag{3.1}$$

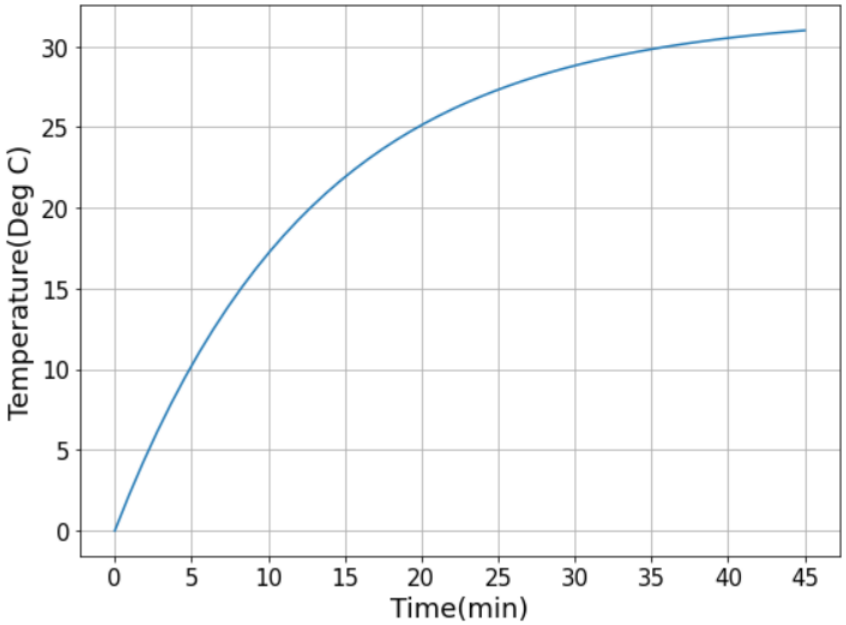

Figure 3.2: Simulated hotspot thermal response due to a DC step of 16.67 A/phase by using the approximated Temperature rise from [4]

However, measurements have also shown a non-linear increase in the thermal steady state values over the range of different DC levels [4]. This is reflected by the asymptotic response of the steady-state temperature vs. GIC, as the hotspot temperature rise does not scale linearly with the magnitude of DC current. With a GIC's signature from Fig. 3.1, the asymptotic behavior can be seen as a series of exponential decay function accumulated above the final steady-state thermal response of respective DC levels. This can be demonstrated by the hotspot rise of transformers with a profile of sustained DC levels for 60 minutes [5], as shown in Fig. 3.3.

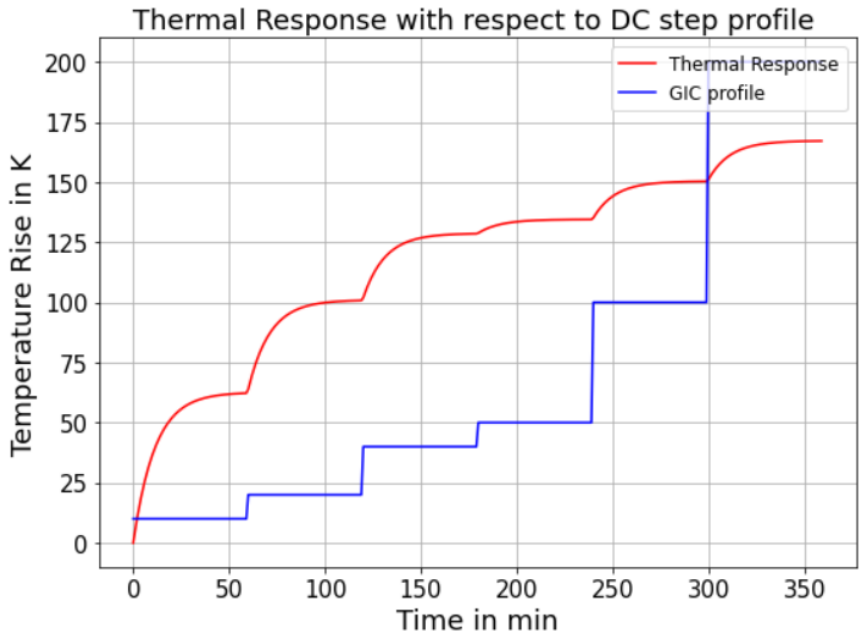

Figure 3.3: Simulated hotspot rise above top-oil for DC profile from [5]

After linearizing this response in the Laplace domain, the time-domain solution was then approximated using the trapezoidal numerical method as follows:

$$y(k+1) = \frac{1}{(1+\frac{2\tau}{\Delta t})}(x(k)+x(k+1)) - \frac{(1-\frac{2\tau}{\Delta t})}{(1+\frac{2\tau}{\Delta t})}y(k) \tag{3.2}$$

where x(k+1) is the present thermal steady state value with respect to the magnitude of GICs at the current time and x(k) is the past thermal steady state value for the previous magnitude of GIC, likewise, y(k+1) is the current hotspot temperature rise and y(k) is the hotspot temperature rise for the previous time step. For programming purposes, this response can be approximated using trapezoidal numerical method. Fig. 3.3 can serve as a validation of the resultant equation implementation for approximating thermal behavior of the transformer against the actual data from [5]. The total hotspot temperature is computed by adding the top-oil temperature to the hotspot temperature rise as follows:

$$\theta_{total} = \Delta\theta_{hotspot} + \theta_{top-oil} \tag{3.3}$$

3.2 Factors Affecting Transformer Thermal Capability

Literature has established that transformer's sensitivity to DC is influenced by its design parameters including core type, type of transformer (Generator Step-up vs. autotransformer), number of DC-carrying turns on the windings and voltage rating [3]. For example, single-phase power transformers are statistically proven to be more susceptible to GICs than the three-phase transformers, while three-leg core type transformers are the least susceptible [27]. Prior work [5] has produced 40 different types of design-specific transformer models to investigate the aforementioned consequences of GICs on the thermal behavior of transformers. This study also explored the variations in thermal response with respect to different geometries of tie-bar. The work for this thesis utilizes as its starting place the models developed in [5].

The hotspot temperature rise of a winding is different from that of metallic part (e.g., tie bar) due to different thermal time constants, for the same GIC signature. Results from previous work have demonstrated that tie-bars located near the core are the most thermally-stressed components in transformer, under the influence of increased DC current injection due to GICs [28],[29]. The total hotspot temperature is computed by adding the top-oil temperature to the hotspot temperature rise.

4. CASE STUDIES ON TRANSFORMER THERMAL ASSESSMENT

4.1 Scenario Description

Since the information regarding the actual grids is protected as Critical Energy Infrastructure Information (CEII), Texas A&M university has developed publicly available synthetic grids for research and educational purposes.The process involved in building these models are described in [30]. These models are situated on a real geographic footprint, therefore realistic in function; however, do not contain any non-public data. ACTIVSg2000 [31]—a 2000 bus case on the footprint of Texas— is used to test the proposed approach.

For the first case study, the time-varying Electric field derived from NERC benchmark event of March 13, 1989 [25] is used as an input to the 2000 bus synthetic case to develop the GIC model for the system. Even though the benchmark event refers to the recorded observations from the Ottawa observatory, the latitude scaling according to the geomagnetic latitude of Texas is ignored; this is equivalent to applying geoelectric amplitudes associated with the resistive Quebec model to a different geographic area. The reason is to focus on the response of the grid to a severe space weather scenario irrespective of the geographic location. The Electric field data has a sampling rate of 6 seconds with a maximum E-field reaching up to 8 V/km. The time constant is derived from [5] and is set to 460 seconds. The steady-state temperatures for Design 2 of the tie-bar were selected to investigate the extreme condition of maximum thermal response.

Thermal time constant plays an important role in how the tie-bars will behave to the flow of current. The smaller the time constant, the earlier the tie-bar's temperature will approach the steady-state value for the respective GIC current. These 40 design types of transformer thermal models do not account for steady-state temperatures for GICs more than 200 A/phase. However, when the 1989 Benchmark event and its derivative events are applied as inputs to a system-wide transformer temperature analysis, the GICs are found to reach as high as 350 A/phase in the neutrals of a few transformers. In order to accurately predict the hotspot temperature rise for GICs of

higher magnitude than 200 A/phase, the thermal assessment model is modified by integrating the steady-state temperature for 1000 A/phase which is accomplished through interpolating the preceding gradient. This reflects the possible upper bound of the steady-state temperature if the GICs reached 1000A/phase. This process of interpolation was carried out for all 40 different models. Fig. 4.1 shows the steady-state hotspot temperature rise vs. GICs/phase derived from T1 thermal model from [5], modified with an additional entry of an estimated temperature rise corresponding to 1000 A/phase.

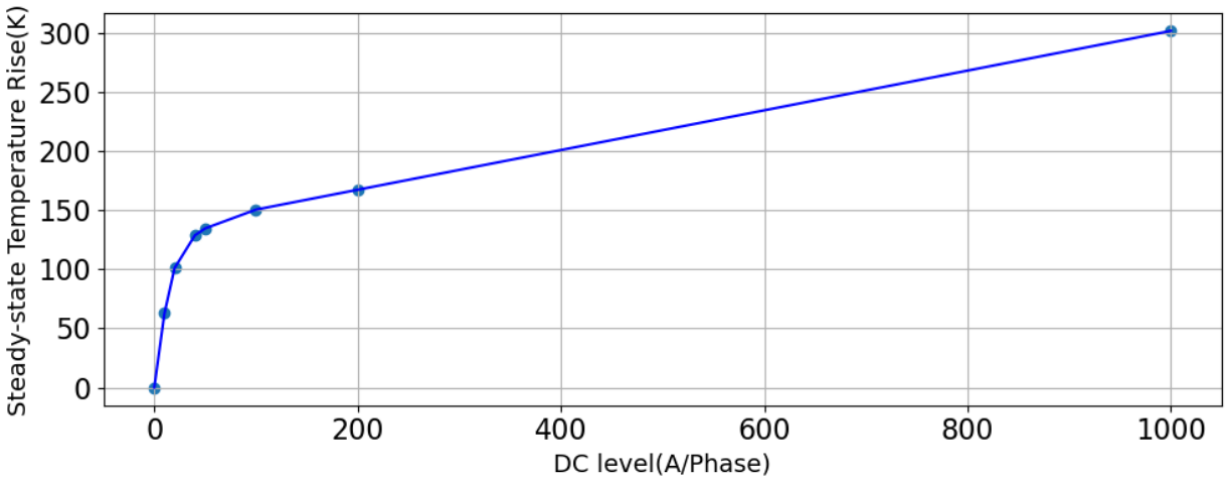

Figure 4.1: Interpolated hotspot temperature rise for 1000A/phase

The second case study simulates the effects of electric field's direction on the magnitude of GICs in the bulk power system and its thermal repercussions on transformers. The time-varying electric field is rotated by a total of 4 different angles—45 degrees, 90 degrees, 135 degrees and 180 degrees— with the idea that the linear relationship between Eq. (2.4) and Eq. (2.5), would result in same magnitude of GICs flowing in the opposite direction for pair of angles such as 0 and 180 degrees, 90 and 270 degrees, etc. In order to visualize the Geographic Data View (GDV) plots, the maximum effective GICs/phase for each storm's rotation is calculated using a single snapshot, peak Electric field of 8 V/km, as a worst case scenario.

The objective of the third case study is to investigate the footprint of the duration of GICs

on the hotspot temperature rise of the structural part of transformers. The sampling rate of the NERC Benchmark Event is scaled from 6 seconds to 12, 20 and 40 seconds while keeping the time constant of the tie bar constant at 480 seconds for each NERC benchmark event derivatives.

For the fourth case study, an analysis of the effect of electric field's magnitude on the transformers is presented. The scaling factors—2 and 0.5—are applied on the time-series Electric field of NERC benchmark event resulting in peak electric fields of 16 V/km and 4 V/km, respectively.

The time series waveshape of effective GIC/phase for every transformer will vary depending on the location within the network and the configuration of the circuit, irrespective of the same reference event. Therefore, the resulting GIC time series, GIC(t), is calculated for each transformer, for a total of 861 transformers in this study. A majority of the GSU transformers are rated 115 kV, while some are rated at 230 kV and 500 kV. The transformer thermal response tool is developed in python environment. The corresponding GIC(t) for each transformer is applied as the input to the transformer thermal model which calculates the time-series hotspot temperature rise of tie-bars for all the transformers included in the interconnection-wide model, with respect to different models from [5].

Transformers' tie-bars reaching maximum instantaneous hotspot temperature rise were evaluated against the temperature limits of 180°C and 160°C for structural parts and windings, respectively [8]. As shown in Table 4.1, transformer's susceptibility to GICs depend on the condition of the transformer which is reflected by the amount of years the transformer has been in service. Table 4.1 was used for the assessment to identify transformers that could potentially have thermal impacts.

This framework of identifying the transformers that can potentially violate the temperature limits combined with studying the respective peaks of GICs/phase is used to present the approximate threshold of peak instantaneous GICs magnitude. Although all the transformers in the case study were assumed to be described by one of the 40 different transformer models outlined in [5], the individual specific technical data of the transformers from the case study is not considered while calculating the hotspot temperature rise, which can give rise to uncertainties. The hotspot tem-

Table 4.1: Categorising transformers based on condition-based GIC susceptibility [8]

Parameter	**Condition-Based GIC Susceptibility Criteria**		
	I	II	III
Age	0-25	25-40	>40
Hotspot Temperature Limit for Structural Parts (°C)	180	160	140

perature during a real GMD event is anticipated to be accurately reflected by at least one of the transformer models. Fig. 4.2 shows the proposed architecture for transformer thermal assessment subjected to several environmental factors involved in the generation of GICs.

4.1.1 Scenario 1: Analysis of 1989 NERC Benchmark Event

Having calculated the effective GICs per phase for all transformers as inputs to 40 different thermal models, the hotspot temperature rise is computed. T24 was identified as the most thermally vulnerable transformer model during the study, owing its high temperature rise to a very high number of turns of N = 1467 in the HV-winding [5]. Fig. 4.3 helps in visualizing transformers' hotspot temperature simulated with worst-case model(T24) along with its corresponding GICs. This study was carried out with 1989 NERC Benchmark event. Only the transformers that violated the temperature limit of 180°C were selected (which are 18 in this case).

Fig. 4.4 demonstrates the instantaneous total hotspot temperature at the transformer's tie-plate simulated with T24 transformer model with respect to the corresponding GIC profile. It can be noticed that the GICs/phase reaches the maximum value of 334.5 A. According to T24 model, the steady-state value of the temperature rise with a 200 DC current injection is 213.4 K. Considering that even when the GICs were as high as 334.4 A/phase, the tie-bar only reached a hotspot rise of 143.26 K; this signals that the duration of GICs/phase of a very high current peak was much less than the thermal time constant of the tie-bar. This transformer violates the maximum thermal threshold for category 1.

The total number of transformers that violated the temperature threshold for structural parts

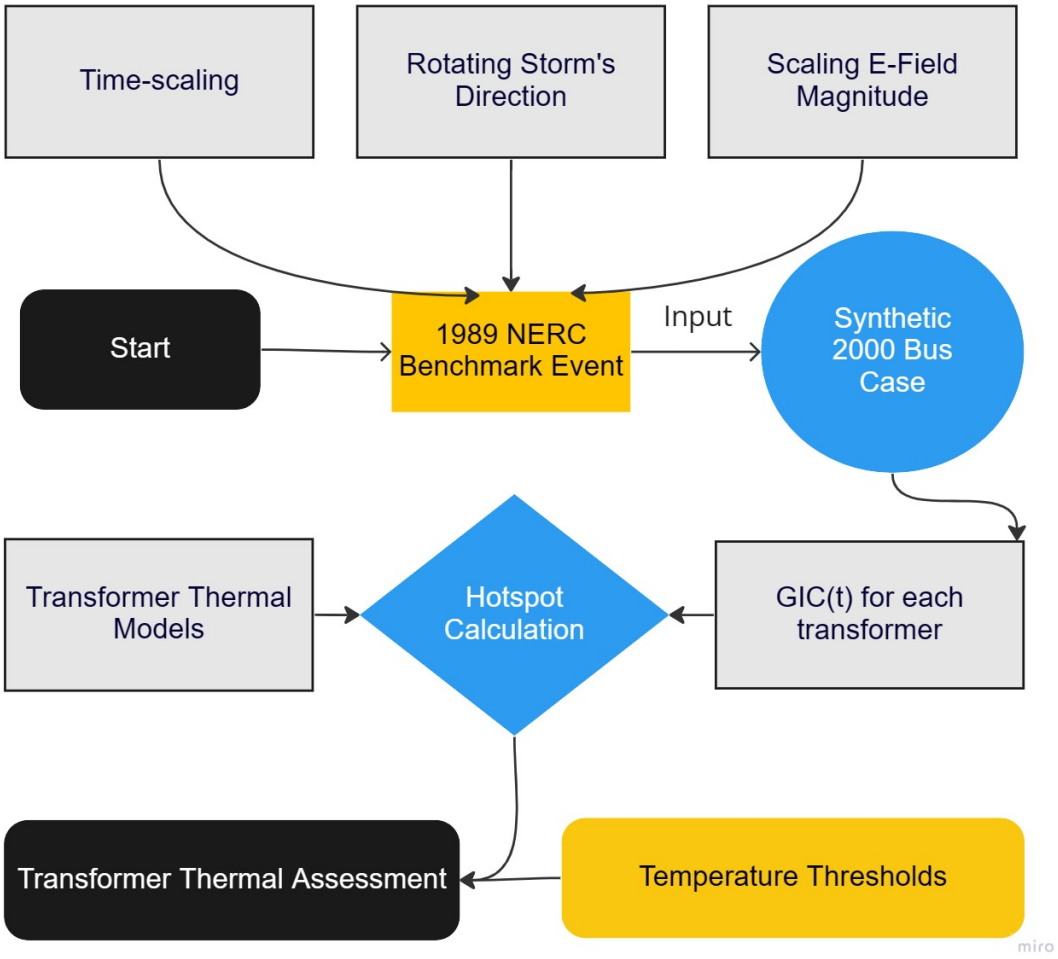

Figure 4.2: The proposed framework for transformer thermal assessment for GMD events subjected to several environmental factors.

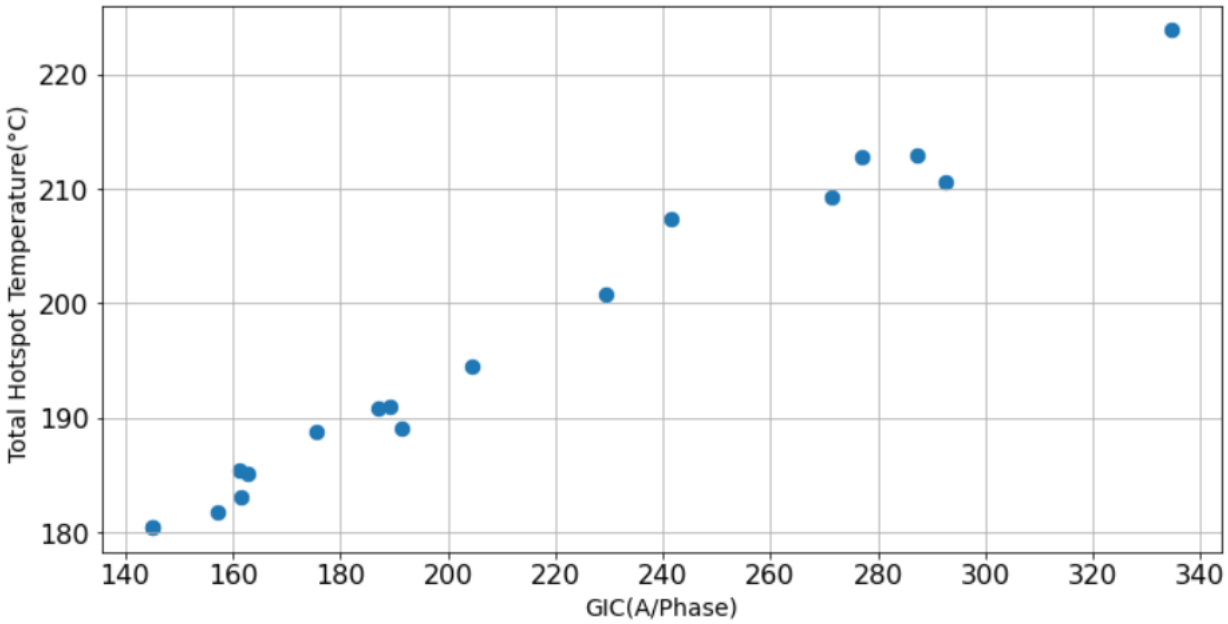

Figure 4.3: Total hotspot temperature and the corresponding GICs for transformers violating the temperature limit for Category 1 simulated with T24 transformer thermal model. [5]

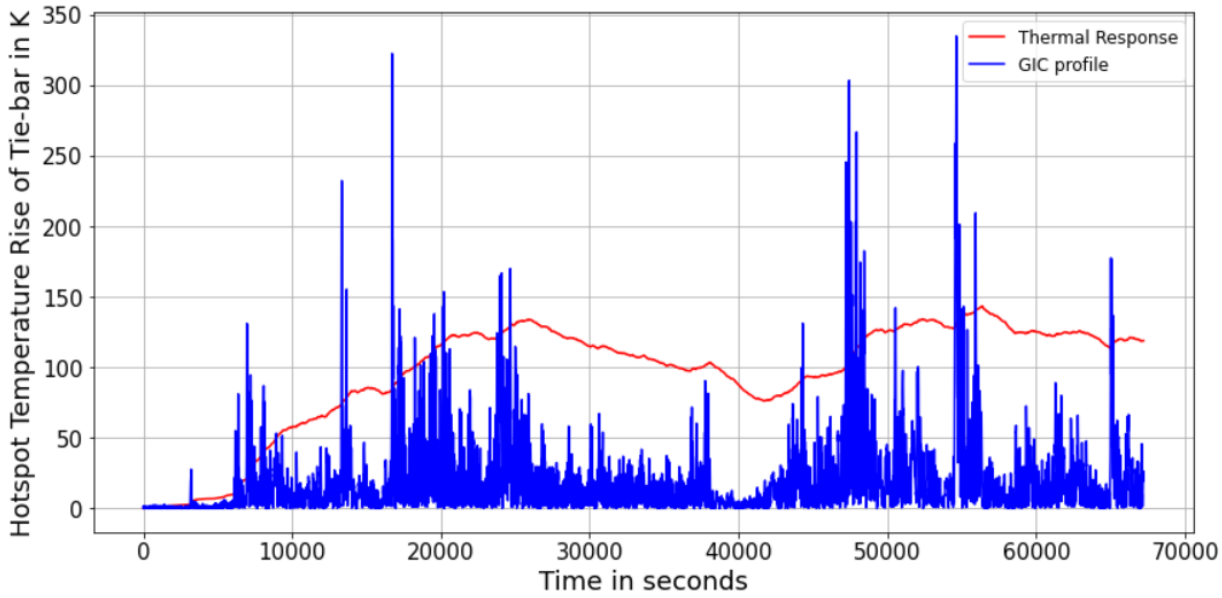

Figure 4.4: Maximum hotspot temperature rise versus time for transformer connected from Bus 18 to Bus 10 using T24 transformer model from [5] , subjected to NERC benchmark event.

are summarised in Table 4.2 according to the condition-based categories of transformers from Table 4.1. These results take simulation results from all transformer models into account. It was concluded that T24 model contributed the most number of transformers that were violating the hotspot temperature limits. Even with the worst-case scenario, almost 17% of transformers have a high degree of susceptibility to effects of GICs with respect to Category I. Correspondingly, almost 29% of transformers are susceptible for category II, and 43% of transformers contribute to GIC susceptibility for Category III.

Table 4.2: Total number of transformers violating the temperature threshold for structural part subjected to NERC Benchmark Event

Condition-Based GIC Susceptibility Criteria	**Number of Transformers**	
	All 40 Transformer Thermal Models	T24 Transformer Thermal Model
Category I	505	153
Category II	1242	254
Category III	2814	374

4.1.2 Scenario II: Directional Sensitivity to GICs

The objective of this study is to investigate the directional sensitivity of GICs on transformer's thermal response while observing the transformers that are likely to encounter high neutral currents for multiple storm directions, as mentioned earlier, so that monitoring strategies could be devised accordingly. The storm's direction is rotated clockwise in accordance with the cardinal directions where 0 degrees is North, 45 degrees is Northeast, 90 degrees is East, 135 degrees is Southeast, 180 degrees is South and 270 degrees is West.

The maximum transformer GICs/phase are plotted in a GDV format, which displays the GIC's magnitude across the fleet of transformers using a coloured contour, where the size of oval representing transformers scales in accordance with the GIC's magnitude. For all the scenarios with various storm's direction, the GDV plot is developed by adopting a common scale of reference for

ease of comparison. The input current is mapped on the GDV plot using scaling ratios of 0, 20000 and 45000 applied on the minimum, median and maximum values of the transformer's GICs/phase, respectively. For instance, a median GIC current of 100 A/phase is scaled to 20000 times its actual size in the contour.

An electric field aligned in the direction that corresponds to the orientation of most of the transmission lines in a network configuration, would yield relatively larger GICs when compared to other directions [32], [33].It is observed that out of all the studied directions on the 2000-bus synthetic electric grid, the 45° rotation of the temporal electric field resulted in maximum GICs up to approximately 344 A/phase, while the peak GIC observed with no rotation was 335 A/phase. Not only did the magnitude of GICs vary with respect to the storm's rotation, but so did the location of the transformers that encountered maximum GICs, as shown in Fig. 4.5 and Fig. 4.6.

The GDV plots for storm's direction rotated by 135° and 180° is shown in Fig. 4.7 and Fig. 4.8.

In this study, the 1989 NERC Benchmark storm's direction was rotated from 45 to 270 degrees, with GICs calculated for each scenario. Once the GICs are calculated, the transformer thermal response is assessed in the next step. Firstly, the results using all 40 transformer thermal models are examined, as shown in Table 4.3. This table demonstrates that with the change in storm's rotation, there were more or less very similar number of transformers violating the 3 different categories for temperature threshold.

Table 4.3: Total number of transformers violating temperature threshold using all 40 transformer model

Storm's Rotation	**Category 1**	**Category 2**	**Category 3**
θ_t	505	1242	2814
θ_t+45	443	1197	2805
θ_t+90	466	1225	2781
θ_t+135	507	1264	2822
θ_t+180	505	1242	2814
θ_t+270	466	1225	2781

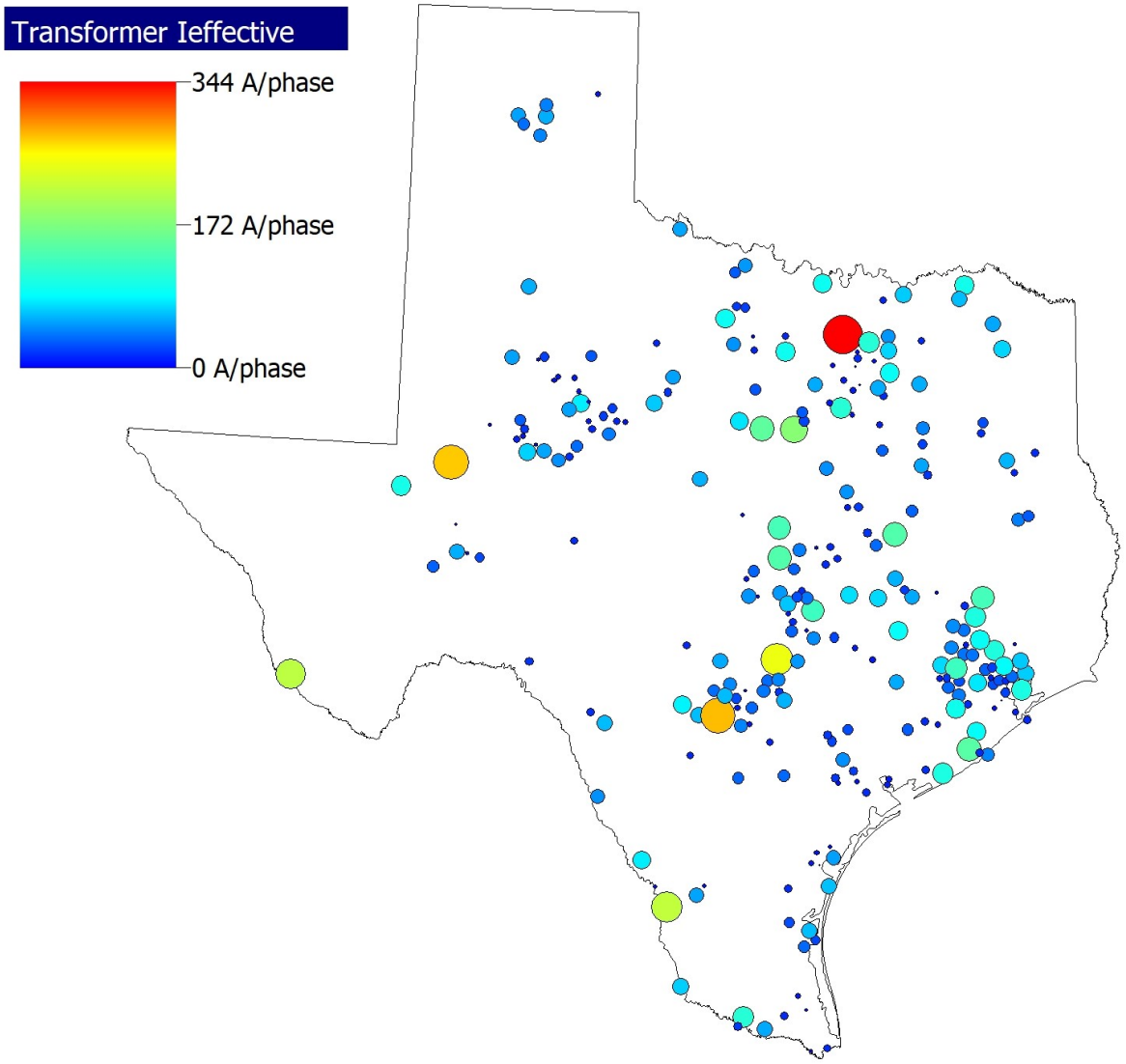

Figure 4.5: GDV plot of the Texas 2k region for 1989 storm's direction rotated by 45°. The contoured plot along with the size of each oval corresponds to GIC's magnitude in transformer's neutrals.

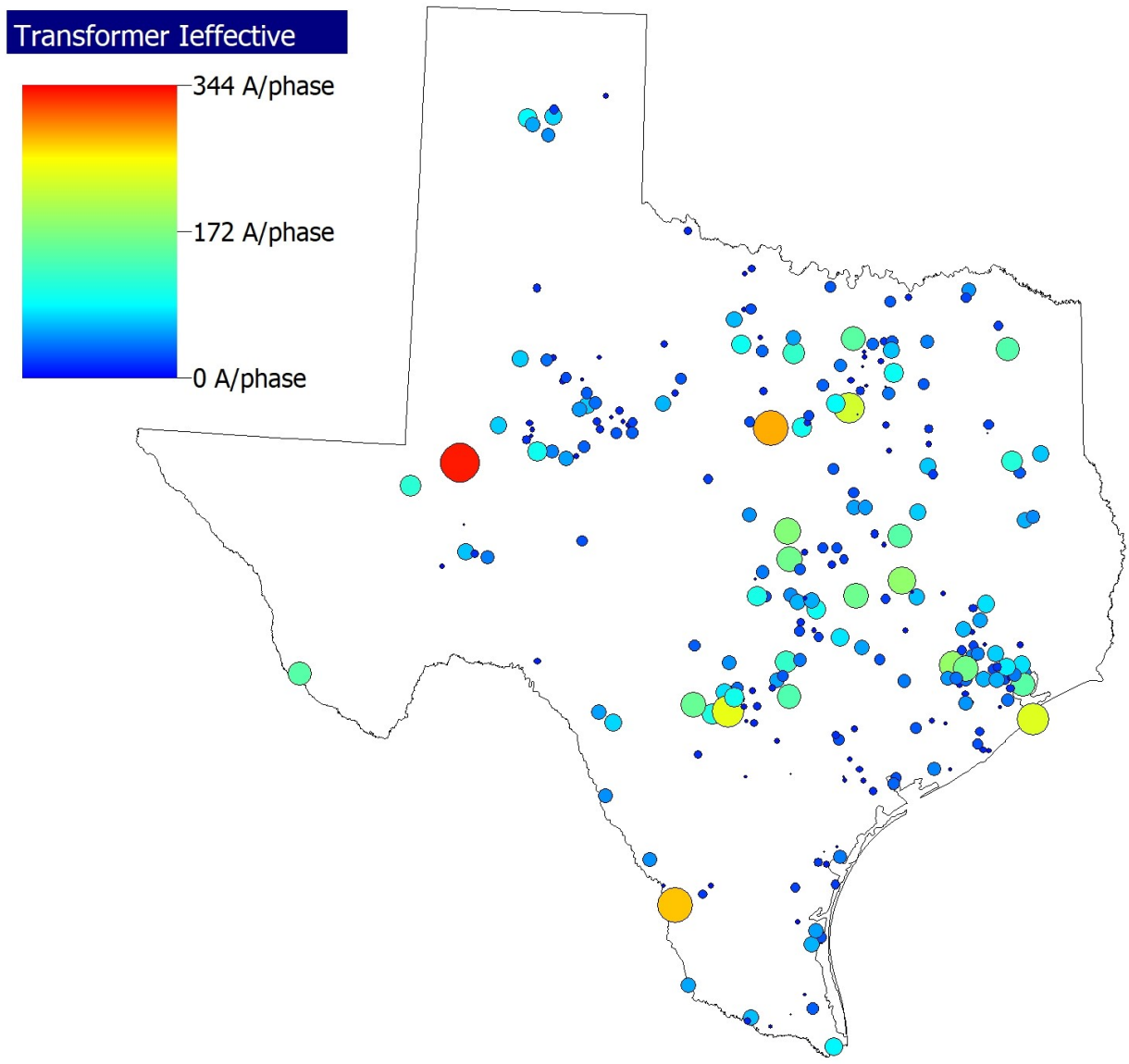

Figure 4.6: GDV plot of the Texas 2k region for 1989 storm's direction rotated by 90°. The contoured plot along with the size of each oval corresponds to GIC's magnitude in transformer's neutrals.

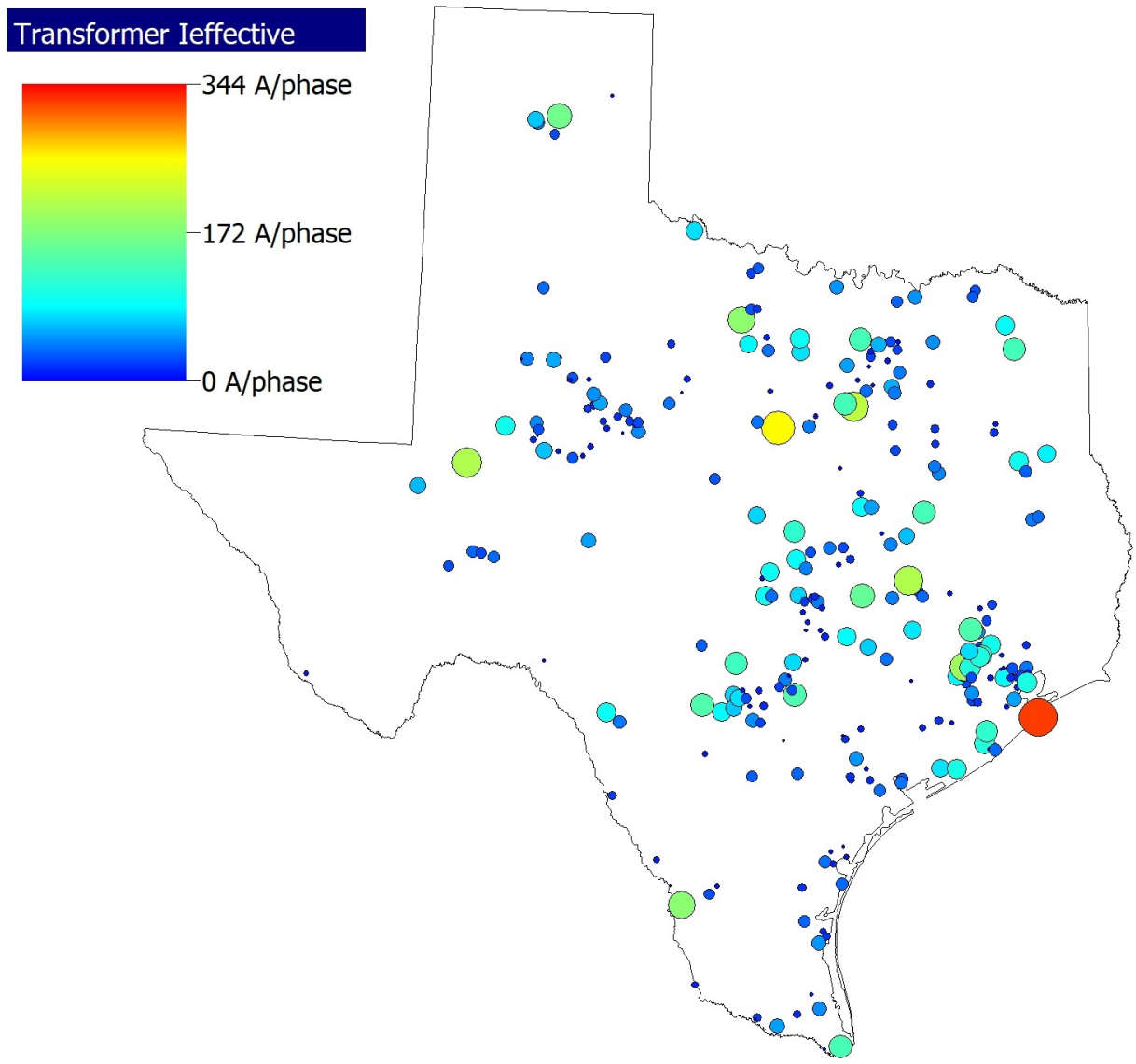

Figure 4.7: GDV plot of the Texas 2k region for 1989 storm's direction rotated by 135°. The contoured plot along with the size of each oval corresponds to GIC's magnitude in transformer's neutrals.

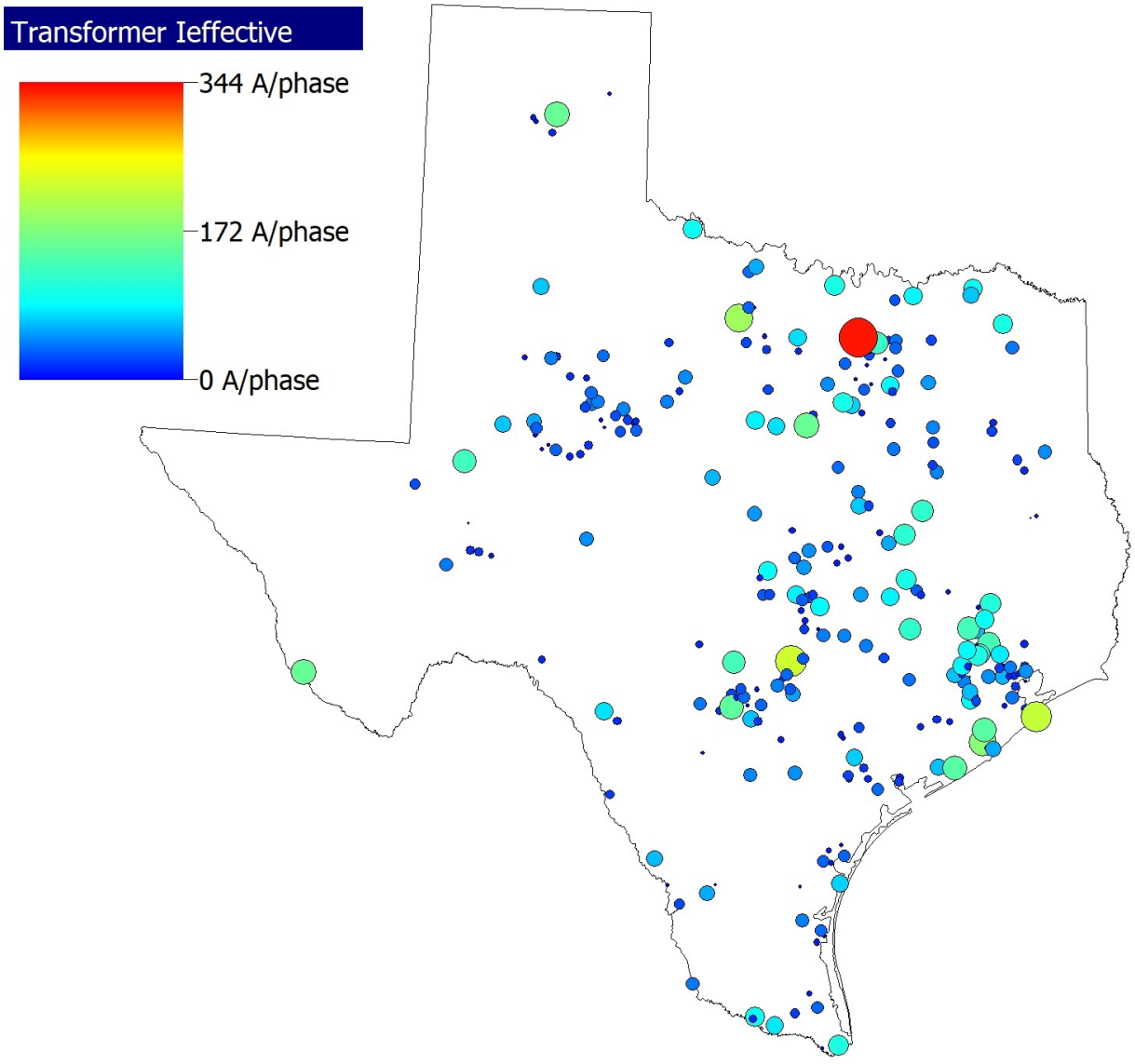

Figure 4.8: GDV plot of the Texas 2k region for 1989 storm's direction rotated by 180°. The contoured plot along with the size of each oval corresponds to GIC's magnitude in transformer's neutrals.

In order to maintain consistency with the interpretation of these results and previous studies of worst-case scenarios, we implemented just the T24 transformer model on the entire transformer fleet. Table 4.4 summarises the sum of transformers violating different category-based temperature thresholds with respect to various modified storm directions. θ_t denotes the 1989 NERC benchmark event's direction at each discrete time step, where t ranges from 0 seconds to 67194 seconds, with a sampling rate of 6 seconds. The similarity of results for the pair of angles such as: θ_t and θ_t+180, θ_t+90 and θ_t+270 reinforces the concept of linearity between Eq. 2.5 and 2.4.

Table 4.4: Total number of transformers violating temperature threshold using T24 transformer model with respect to different degrees of rotated storm

Storm's Rotation	**Category 1**	**Category 2**	**Category 3**
θ_t	153	254	374
θ_t+45	146	251	384
θ_t+90	148	265	372
θ_t+135	148	269	362
θ_t+180	153	254	374
θ_t+270	148	265	372

4.1.3 Scenario III: Analysis of Time-Scaled GMD Events

The duration of GIC flow can impact the transformer's thermal capability to GICs; therefore it's of prime importance to explore time-scaled electric fields. These transformed time-scaled scenarios are intended to provide an example of an extreme event without portraying any historical GMD data. By doing so, we examine the probable impacts of the electric field sampled at a lower time resolution, to simulate GMD events with longer periods of sustained GICs in transformer neutrals.

Considering the magnitude of time-series electric field is unvaried, the resulting GICs have the same magnitude of effective GICs/phase throughout the spectrum of time-scaled GMD events. This ensures to highlight the sensitivity of transformer's heat analysis to the duration of GICs, exclusively. Table 4.5 below shows the potential number of thermally vulnerable transformers

Table 4.5: Total number of transformers violating the temperature thresholds for GIC's condition-based categories for time-scaled GIC events

Time-Scaled NERC Benchmark Event (seconds)	**Number of Transformers Violating Condition-Based GIC Susceptibility Criteria**		
	Category I	Category II	Category III
6 (original)	505	1242	2814
12	435	2123	4452
20	1532	3313	6215
40	3136	5682	8919

using all 40 transformer thermal models. Considering a transformer fleet of 861 transformers, with a cumulative number of transformers of 34,440 for the case study with all 40 transformer thermal models combined; the results in this table are out of 34,440 total transformers.

The worst-case scenario is simulated again by implementing T24 transformer model on entire transformer's fleet; this provides the same metric of comparison with other GMD storm scenarios.

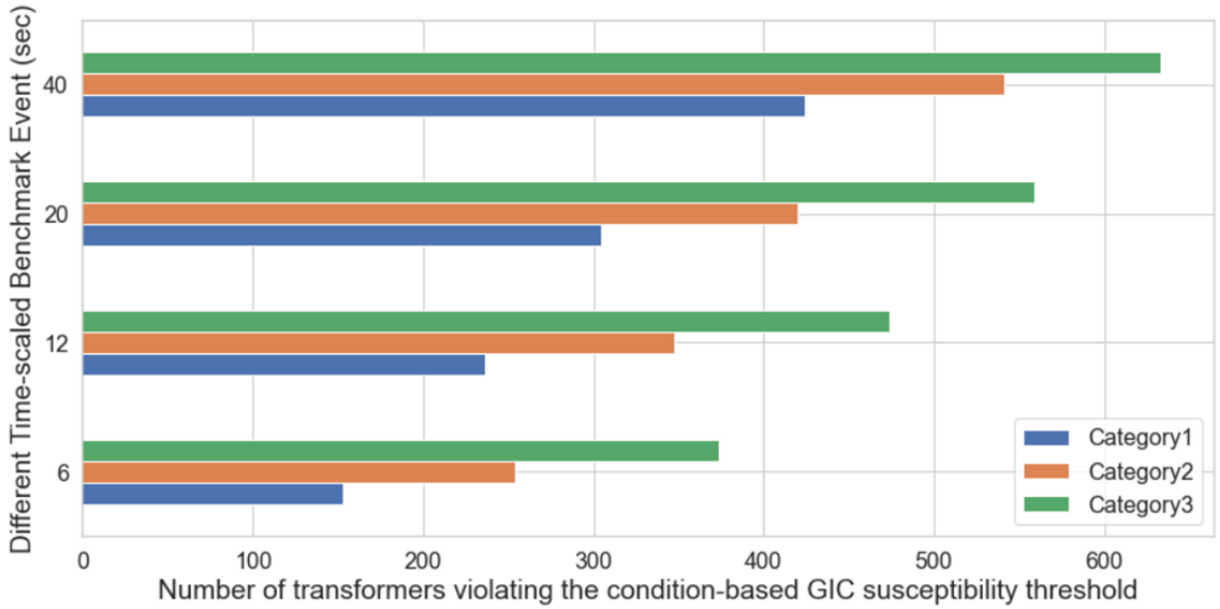

Figure 4.9: Total number of transformers violating the condition-based temperature limits using T24 transformer model with respect to different time-scaled NERC benchmark event.

Fig. 4.9 is used to illustrate the impact of time-scaled reference events on the hotspot temperature rise, and therefore, the number of transformers violating condition-based categories of temperature from a fleet of 861 transformers. As the duration of GICs is incremented from 6 seconds to 40 seconds, there is a noticeable increase in the total number of possible transformer temperature violations—by a factor of 14.461 in the case of category 1.

4.1.4 Scenario IV : Transformer Thermal Capability and Variations in Storm Intensity

The storm intensity of the NERC benchmark event is doubled and halved by scaling the magnitude of the time-series electric field accordingly. These synthetic scaled events can facilitate in performing a comparative analysis of different storm intensities and the thermal susceptibility of transformers. The time resolution from storm to storm is kept constant at 6 seconds. After applying the scaled electric fields on the 2000-bus synthetic grid, it was observed that twice the electric field induced twice the voltage and current, and vice versa. Fig. 4.10 shows the simulated current in the transformer neutral connected from Bus 18 to Bus 10 under different scaled GMD events.

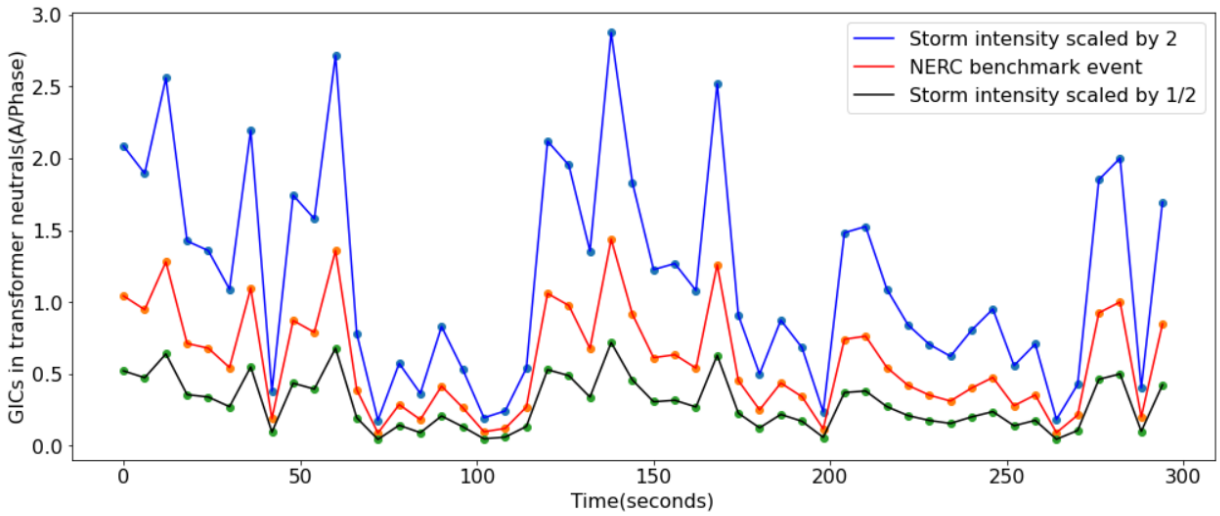

Figure 4.10: Effective GICs/phase in a transformer neutral connected from Bus 18 to Bus 10 for different storm's intensity.

After procuring GIC flows in the transformer's neutrals using scaled geoelectric field as input,

the susceptibility of transformers is examined using all transformer thermal models.

Table 4.6: Variation in storm's intensity and transformer thermal assessment using T24 transformer thermal models

Scaled Intensity of NERC Benchmark Event (V/km)	**Number of Transformers Violating Condition-Based GIC Susceptibility Criteria**		
	Category I	Category II	Category III
NERC Benchmark Event	153	254	374
Scaled by 2	332	456	608
Scaled by 1/2	37	100	196

Considering the contribution of T24 model to the sum of probable susceptible transformers is the highest, thermal behavior of transformer fleet is simulated specifically by adopting T24 transformer model, as used previously. The results for transformer thermal assessment for this study are shown in Fig. 4.11 and Table 4.6. From this analysis, we can conclude that electric field intensity has direct proportionality with the number of possible transformer's thermal damage. With the peak Electric field of 16 V/km for storm's intensity scaled by 2, maximum GICs as large as 668.9 A/phase can flow in transformer's neutrals connected from bus 18 to bus 10 and the predicted tie-plate total hotspot temperature exceeds 180°C twice; once for approximately 100 minutes during the first set of GIC peaks and for 180 minutes for the second (plot not shown). This increased level of GICs can introduce a higher infrastructure risk since transformers can be more vulnerable or resistant to high magnitude of DC current, depending on their types and configurations.

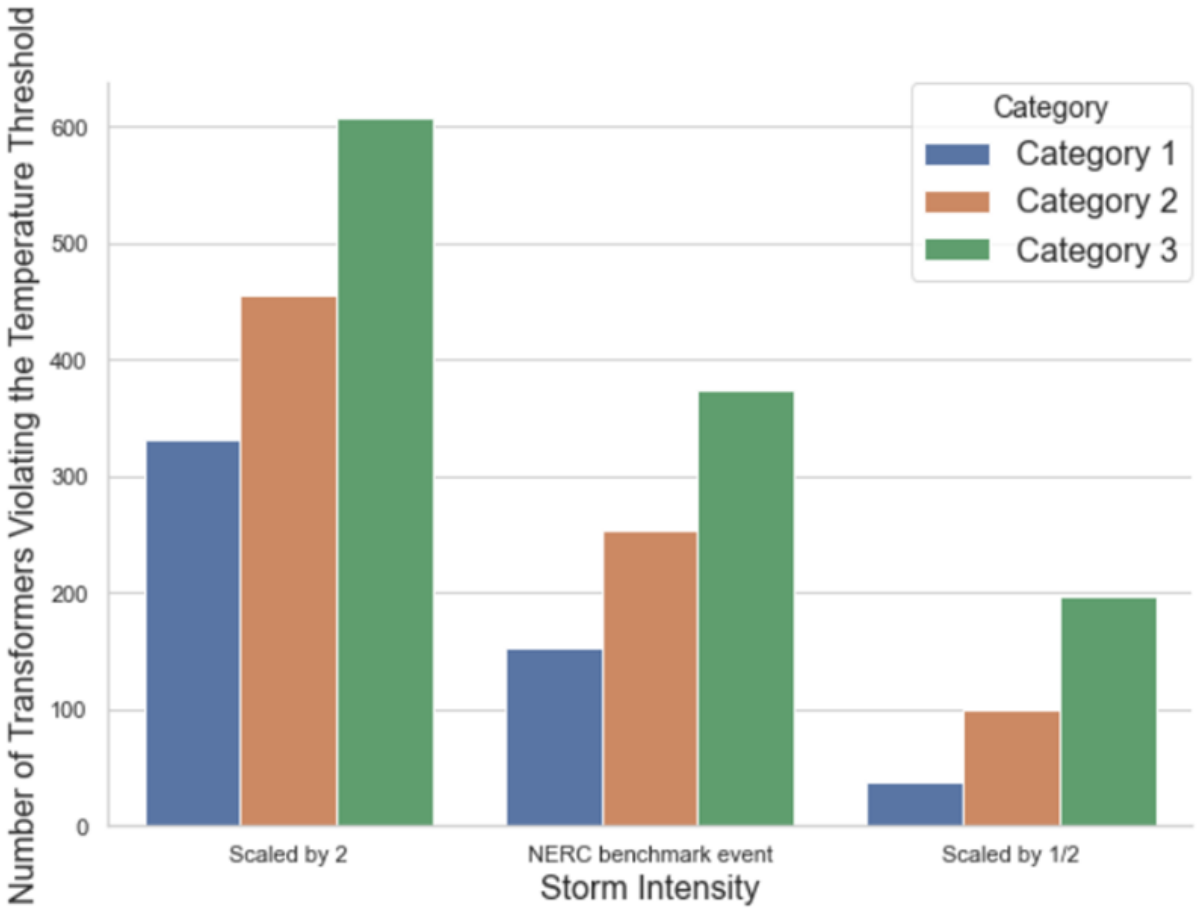

Figure 4.11: Number of transformers violating the condition-based categories for temperature thresholds based on the reference and scaled storm intensity of NERC benchmark event.

5. CREATION AND APPLICATION OF SYNTHETIC GMD STORM ON TRANSFORMER THERMAL ASSESSMENT

5.1 Creation of Synthetic GMD Storm

This part of the research focuses on creating synthetic GMD with varying storm intensities with the goal of testing the resiliency of the power system. Even though GMD data can be obtained from magnetometer observatories, there is a very limited set of strong GMD data available. The last severe GMD event characterized by a K-index of 9 that resulted in major disruptions to the Quebec power grid happened on March 13th, 1989. The scarcity of severe storm data of such magnitude as of 1989's has necessitated the development of synthetic storms.

By using publicly available geomagnetic storm data derived from the NERC Benchmark event of 1989 comprising of the non-uniform electric field, synthetic GMD storms can be generated. Even though the benchmark event refers to the recorded observations from the Ottawa observatory, the latitude scaling according to the geomagnetic latitude of Texas is ignored; this is equivalent to applying geoelectric field amplitudes associated with the resistive Quebec model to a different geographic area. The reason is to focus on the response of the grid to a severe space weather scenario irrespective of the geographic location. We select the observed storm developed statistically by NERC as a starting point for two major reasons. Firstly, because it captures the true variability of a GMD storm and secondly, it also reflects the time duration of the storm which is an important factor in the analysis.

Different fragments of the Electric field data from the reference event are chosen at random, which then undergo temporal and spatial variations achieved by scaling the time duration, magnitude, and direction of the storm. The statistical outcomes from [34] support the linear scaling of the reference storm used in this work. The severity of the storm can be modified by applying various combinations of scaling factors, again selected at random from the normal distribution to the aforementioned parameters of the storm. A random scaling factor is chosen from a uniform

probability density function which is selected from a range specified by upper and lower limits. Therefore, the outcomes of the resultant factor are equally likely. The upper and lower limit is selected in accordance with the parameter that is scaled. The modified fragments of the storm are then concatenated into a new dataset that represents a synthesized GMD storm.

5.1.1 Transformation Matrices for Fragments

A fragment of variable size is selected from the reference electric field dataset; the starting index of the fragment is chosen at random from a uniform probability density function. Each fragment goes through the following transformation:

5.1.1.1 Temporal Variation

Since the duration of GIC flow can affect the thermal capability of transformers, the sampling rate is scaled by a scaling factor chosen at random from a range of 0.5 and 2. This simulates GICs for a longer duration in transformer neutrals if scaled by greater than 1 and vice versa.

5.1.1.2 Variation in Storm's Intensity

The lower and upper bound for the range from which a random scaling factor is extracted is 0.1 and 4, respectively. Time-scaled fragment then undergoes spatial transformation through this function. Since the magnitude of magnetic fluctuations, as determined by historical data, can be four times as severe as the March 1989's event, the upper limit for scaling the NERC Benchmark storm's intensity is selected as 4.

5.1.1.3 Rotation of Storm's Direction

After the fragment was subjected to time-scaling and magnitude-scaling, the storm's direction at each time step is rotated anywhere between 0 and 360 degrees. It is crucial to integrate this spatial variation because the thermal response of transformers is sensitive to the direction of the storm. With respect to the alignment of the transmission lines in the electric network configuration, the direction of electric field can yield different magnitudes of GICs. Another important observation is that the geographical location of transformers experiencing maximum GICs can vary as well [32].

5.1.1.4 Blending of Fragments

To merge two fragments of equal size that have distinct spikes at opposite ends, a technique known as "blending" is utilized. A small subset of these fragments from respective areas of interest is blended according to equal weights given to each subset. This ensures a reduction in the amplitude of spikes in the final dataset.

Finally, through an iterative process, multiple fragments that have been transformed using the previously mentioned parameters are concatenated to form a modified dataset representing electric field data of a fictitious storm. Therefore, the final dataset for different generated fictitious storms may vary given the stochastic nature of the procedure.

5.2 Generation of 100 Synthetic GMD Storms

For initial work, a hundred synthetic GMD storms are generated. Because of the inherent nature of randomness and permutation due to the order of modified fragments, the resultant synthetic storms are unique. In order to quantify the severity of the storm, the peak magnitude of the Electric field of each of the 100 synthetic storms is calculated. Fig. 5.1 depicts a graphical representation of the frequency of distribution of the peak Electric field distribution across 100 generated synthetic storms. For a range of synthetic storms, the y-axis takes in the counts of peak E-field in V/km, which is displayed along the x-axis. The insight obtained from this histogram is that a large number of generated synthetic storms have a peak Electric field in the range of 30-35 V/km. This is obviously much higher than the original storm which has a peak electric field of 8 V/km. But since we are uncertain about what a future GMD storm could look like, therefore our primary objective is to explore a range of potential future storms, many of which are larger than the peak electric field of the original storm in this case. Further analysis of the generated storms shows that the highest recorded electric field was 39.6 V/km, indexed at the 60th storm.

Fig. 5.2 shows a comparison of the Northward component of the Electric field, Ex, of the original storm with one of the synthetic GMD storms. The maximum E-field magnitude reached as high as 12 V/km for the synthetic storm at an earlier onset of the GMD storm.

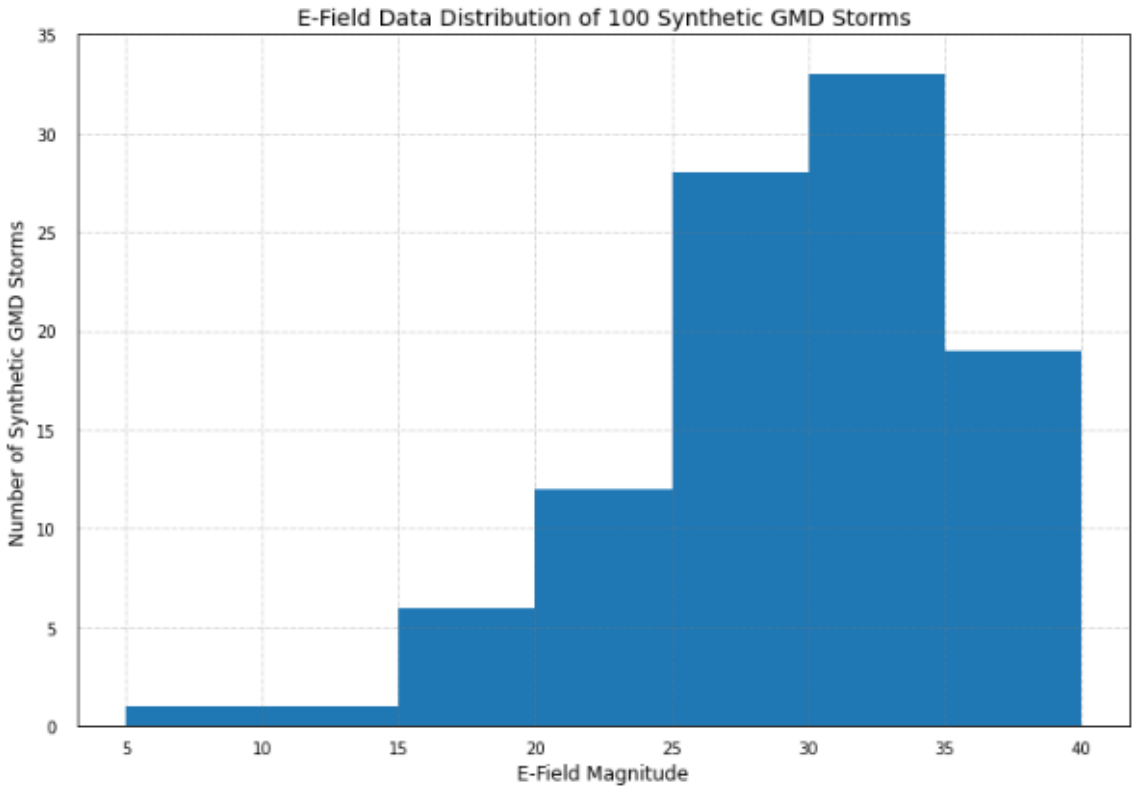

Figure 5.1: The distribution of peak Electric field data for 100 synthetic GMD storms

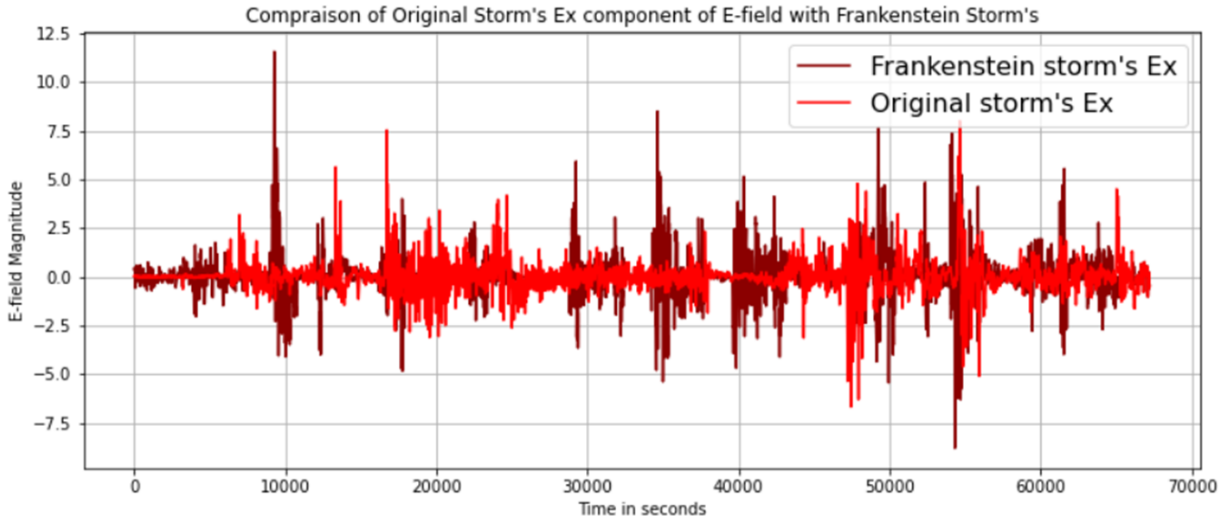

Figure 5.2: Comparison of Ex component of the Electric field of the NERC Benchmark event and the synthetic storm

Likewise, a comparison of Eastward, Ey, component of the Electric field of the reference event and one of the synthetic GMD events is presented in Fig. 5.3. The synthetic GMD storm is also referred to as the Frankenstein storm, as seen on the figure labels.

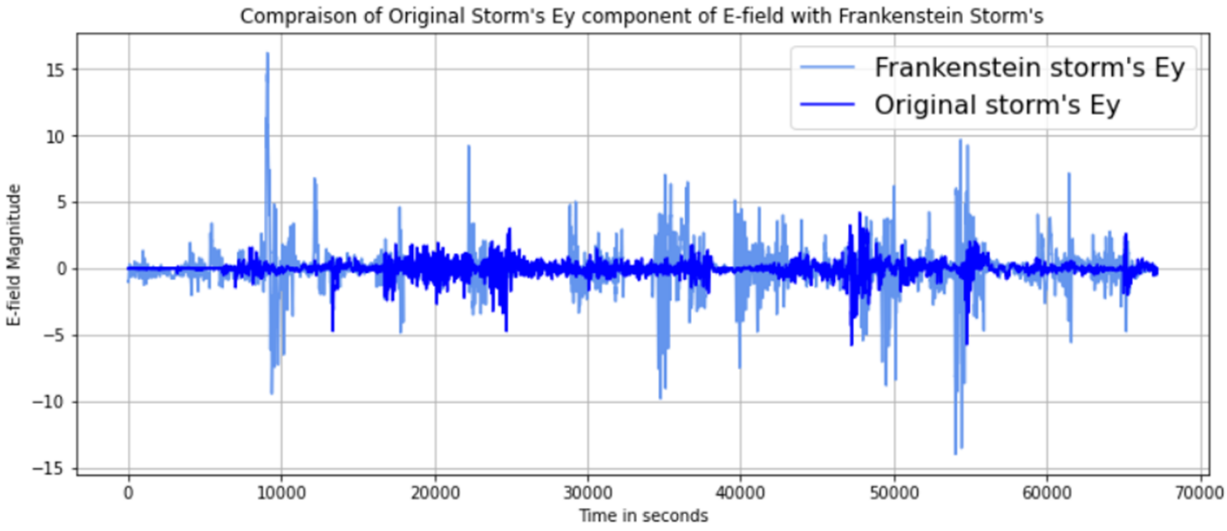

Figure 5.3: Comparison of Ey component of the Electric field of the NERC Benchmark event and the synthetic storm

5.3 Transformer Thermal Sensitivity Analysis to Synthetic GMD Storms

One way of quantifying the extremity of GMD storm's impact on the power grid is by investigating the thermal sensitivity of the transformers to the synthesized geoelectric field in a two-step process. This case study is demonstrated using a 2000-bus, 861-transformer synthetic grid. First, the time series effective GICs/phase, GIC(t), is computed for each transformer that is subjected to all of the synthetic GMD storms. In the second step, the resulting GIC(t) for each transformer is input into the hotspot calculation model which approximates the hotspot temperature rise of tie-bars for a total of 861 transformers according to 40 different transformer thermal models detailed in [5]. Therefore, for each of the 861 transformers in the case study, forty separate time-series thermal simulations were performed.

The transformers under study included GSUs and autotransformers of various nominal voltages

at different locations. It is assumed that at least one of the transformer thermal models from [5], which are based on various technical specifications of transformers, can accurately correlate with a transformer in the fleet.

The results of the maximum total hotspot temperature of the tie-bars were utilized to estimate the number of transformers that could potentially be at risk of thermal damage due to GIC flow. The transformers were screened according to the temperature thresholds based on condition-based GIC susceptibility categories[8], as shown in Table 4.1.

Fig. 5.5 shows the heatmap for the total number of transformers that violated condition-based categories of temperature limits for all 40 transformer models with respect to hundred synthetic GMD storms. For Category I, there was a large number of transformer thermal violations for synthetic GMD storm indexed at 60. The peak temporal Electric field for this particular storm was as high as 39.6 V/km. This implies that for a GMD storm of this magnitude, even the new transformers that have been in service for less than 25 years can be at an increased risk of thermal damage. The information captured from this heatmap can leverage the prediction of possible thermal response for a suite of extreme GMD storm scenarios.

To visualize the response of T24 transformer thermal model with respect to the rest of the models, plots of hotspot temperature rise for a transformer connected from Bus 11 to Bus 10 are simulated with 40 thermal models, as demonstrated in Fig. 5.4. This transformer is subjected to a synthetic GMD storm indexed at 60. Consistent with the study results presented in [5], T24 thermal model is proven to result in maximum hotspot temperature rise, serving as a baseline for the worst-case scenario.

Fig. 5.6 highlights the streamlined thermal assessment of the transformers, where the entire transformer fleet is simulated with just the T24 transformer thermal model throughout the whole study. Even if all of the transformers were brand-new, the results from the most severe GMD storm indexed at 60 revealed that 607 of the 861 transformers that had undergone a time-domain thermal analysis were potentially susceptible to thermal damage, presented by Table 5.1. The evaluation is predicated on the assumption that every transformer in the fleet fits into one of the condition-based

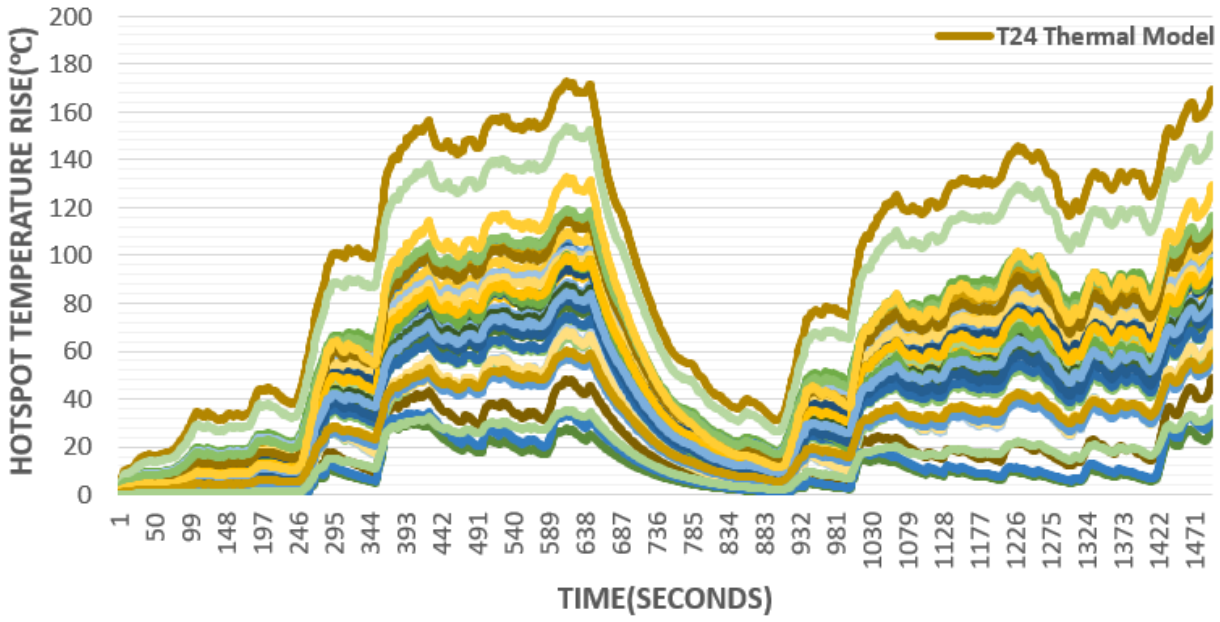

Figure 5.4: Time-series hotspot temperature simulation of a transformer using all 40 thermal models from [5]

GIC susceptibility categories. That said, this necessitates the scope of future study on the impact of the loss of these transformers—if all of them were to face concurrent damage—on the stability of the power grid.

Table 5.1: Number of transformers violating the temperature limits under a synthetic GMD storm indexed at 60

Condition-Based GIC Susceptibility Criteria	**Number of Transformers**	**% of Total Number of Transformers**
Category I	607	70
Category II	704	81
Category III	760	88

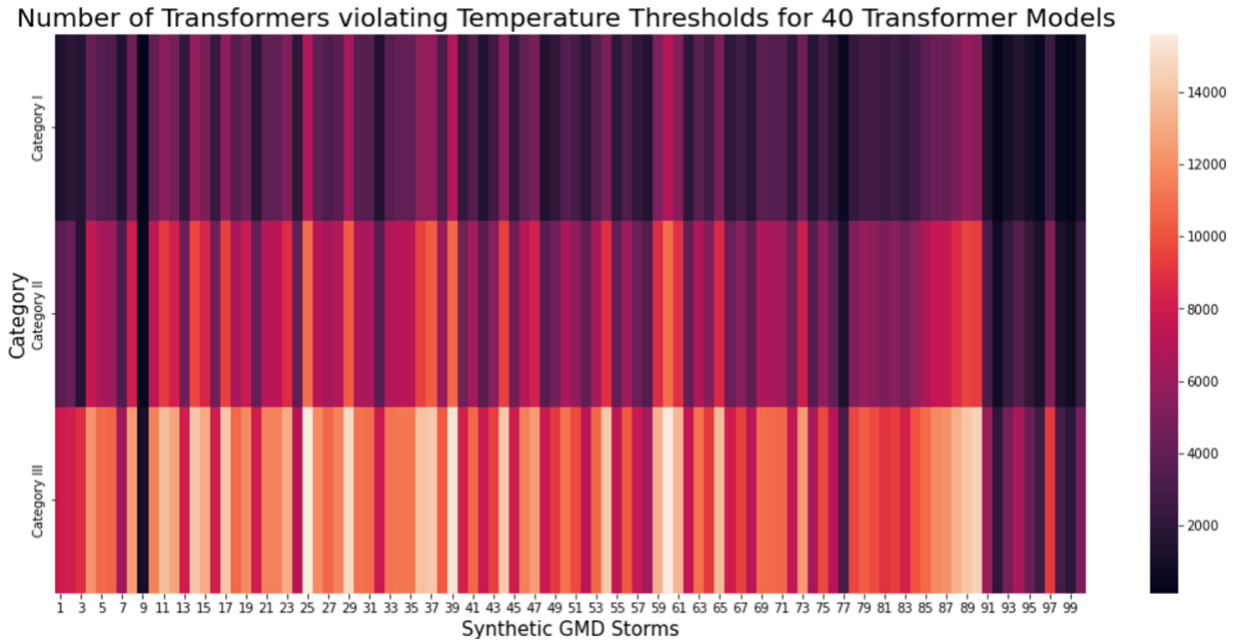

Figure 5.5: Heatmap for the total number of transformers violating the GIC susceptibility temperature thresholds for 100 different synthetic GMD storms

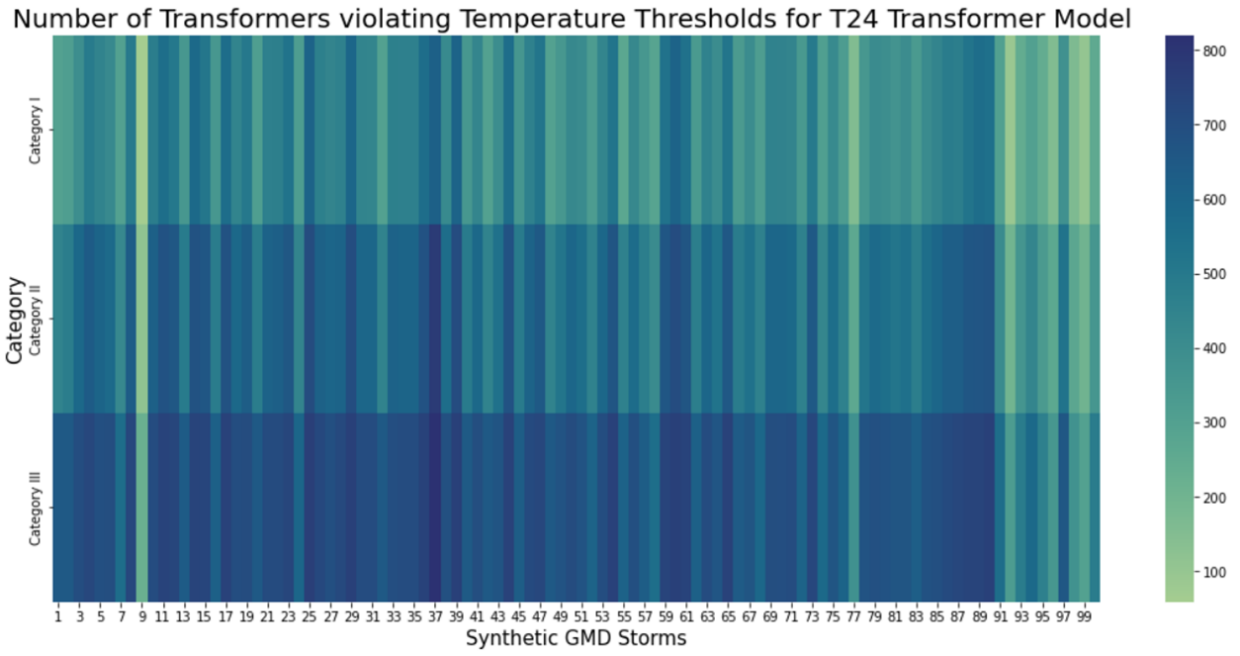

Figure 5.6: Heatmap for the total number of transformers violating the GIC susceptibility temperature thresholds for 100 different synthetic GMD storms simulated with T24 thermal model

6. SUMMARY AND CONCLUSIONS

This thesis has provided an analysis of a large power system-wide transformer thermal assessment under the influence of GICs. The NERC benchmark event is used to derive the GICs/phase for the transformer fleet in a 2000-bus synthetic case. Transformer thermal models based on different technical data are employed to allow a qualified design-specific dynamic thermal response at tie-plate of the power transformers according to the GIC signature for each transformer. The thermal assessment for the transformers is conducted against the total hotspot temperature thresholds of condition-based GICs susceptibility categories of transformers. By modeling the worst-case scenarios of 1989 NERC benchmark event along with its derived synthetic versions of the storm — scaled storm's intensity, time duration and directions — can improve the understanding of the transformer thermal model's impact on power system for heightened system awareness in the possible event of an unprecedented GMD storm.

The scenarios in Section IV offer a means to assess the risk of transformer vulnerability to GMD events for a given storm's direction, duration, and magnitude on the bulk power system. A probable limitation with this presented framework is the existence of uncertainty of thermal response data in the results due to the transformer thermal models not correctly corresponding to the actual transformer type and configuration. This limitation can be accommodated by a systematic application of transformer thermal model on the transformer fleet accordingly.

Section V presents the methodology of constructing extreme synthetic GMD storms and case study results on the thermal sensitivity of transformers to such storms. The synthetic storms can offer temporal GIC series data that would be applicable to other GMD engineering assessments of transformer thermal evaluations as well as steady-state voltage stability studies.

There are many possible avenues for future work. Validating synthetic GMD storms is unquestionably a crucial next step. Principal component analysis, which provides information about the similarity of feature distributions between actual and synthetic datasets, can help with this. Understanding the effects of overall system reliability on an electrical link caused by thermal damage

as a result of extreme GMD episodes is another direction of future research. By developing informed operational techniques or maintaining high-risk bulk power transformers under the safety threshold, that is, by optimizing the transformer loading to lower the danger of transformer thermal repercussions, the negative effects of GICs can be reduced.

The findings of this research can find applications in operational planning and educational research, all with the goal of enhancing the situational awareness and decision-making of large, complex electric grids in the face of an unprecedented extreme GMD scenario.

REFERENCES

[1] "IEEE Guide for Establishing Power Transformer Capability while under Geomagnetic Disturbances," *IEEE Std C57.163-2015*, pp. 1–50, 2015.

[2] "Application Guide: Computing Geomagnetically-Induced Current in the Bulk-Power System," North American Electric Reliability Corporation (NERC), Dec. 2013.

[3] R. Girgis and K. Vedante, "Effects of GIC on power transformers and power systems," in *PES T&D 2012*. IEEE, 2012, pp. 1–8.

[4] "Transformer Thermal Impact Assessment White Paper." North American Electric Reliability Corporation (NERC), Dec. 2014.

[5] "Transformer Thermal Impact Assessments for DC Withstand Capability: Examining the Impacts of Geomagnetically Induced Current (GIC) on Transformer Thermal Performance." EPRI, Palo Alto, CA: 2019. 3002017708.

[6] [Online]. Available: https://www.swpc.noaa.gov/products/planetary-k-index

[7] V. Albertson, B. Bozoki, W. Feero, J. Kappenman, E. Larsen, D. Nordell, J. Ponder, F. Prabhakara, K. Thompson, and R. Walling, "Geomagnetic disturbance effects on power systems," *IEEE transactions on power delivery*, vol. 8, no. 3, pp. 1206–1216, 1993.

[8] "Magnetohydrodynamic Electromagnetic Pulse Assessment of the Continental U.S. Electric Grid: Geomagnetically Induced Current and Transformer Thermal Analysis." EPRI, Palo Alto, CA: 2017. 3002009001.

[9] "March 13, 1989 geomagnetic disturbance," North American Electric Reliability Corporation (NERC), April 2014.

[10] V. D. Albertson, J. M. Thorson, R. E. Clayton, and S. C. Tripathy, "Solar-Induced-Currents in Power Systems: Cause and Effects," *IEEE Transactions on Power Apparatus and Systems*, vol. PAS-92, no. 2, pp. 471–477, 1973.

[11] J. G. Kappernman and V. D. Albertson, "Bracing for the geomagnetic storms," *IEEE spectrum*, vol. 27, no. 3, pp. 27–33, 1990.

[12] W. Naim, P. Hilber, and E. Shayesteh, "Impact of geomagnetic disturbances on power transformers: risk assessment of extreme events and data availability," *Life Cycle Reliability and Safety Engineering*, vol. 11, no. 1, pp. 11–18, 2022.

[13] K. Shetye and T. Overbye, "Modeling and Analysis of GMD Effects on Power Systems: An overview of the impact on large-scale power systems." *IEEE Electrification Magazine*, vol. 3, no. 4, pp. 13–21, 2015.

[14] R. Sharma and J. D. McCalley, "Extreme Value Analysis of Geomagnetically Induced Currents Based on Historical Magnetic Field Data," in *2019 North American Power Symposium (NAPS)*. IEEE, 2019, pp. 1–6.

[15] C. Klauber, K. Shetye, T. J. Overbye, and K. Davis, "A GIC Estimator for Electric Grid Monitoring During Geomagnetic Disturbances," *IEEE Transactions on Power Systems*, vol. 35, no. 6, pp. 4847–4855, 2020.

[16] L. Bolduc, "GIC observations and studies in the Hydro-Québec power system," *Journal of Atmospheric and Solar-Terrestrial Physics*, vol. 64, pp. 1793–1802, 2002.

[17] D. H. Boteler, *Space Weather Effects on Power Systems*. American Geophysical Union (AGU), 2001, pp. 347–352.

[18] J. Kappenman, "Geomagnetic Storms and Their Impact on Power Systems," *IEEE Power Engineering Review*, vol. 16, no. 5, pp. 5–, 1996.

[19] J. G. Kappenman, "Geomagnetic Storms and Extreme Impulsive Geomagnetic Field Disturbance Events – An Analysis of Observational Evidence including the Great Storm of May 1921," *Advances in Space Research*, vol. 38, pp. 188–189, 2006.

[20] "Geomagnetic disturbance monitoring approach and implementation strategies," U.S. Department of Energy, Report, 2019.

[21] "Solar Storm Risk to the North American Electric Grid," Lloyd's and the Atmospheric and Environmental Research, Inc., Report, 2013.

[22] J. Kappenman, "The Evolving Vulnerability of Electric Power Grids," *Space Weather*, vol. 2, no. 1, 2004.

[23] C. T. Gaunt and G. Coetzee, "Transformer failures in regions incorrectly considered to have low GIC-risk," in *2007 IEEE Lausanne Power Tech*, 2007, pp. 807–812.

[24] J. M. Torta, L. Serrano, J. R. Regué, A. M. Sánchez, and E. Roldán, "Geomagnetically induced currents in a power grid of northeastern spain," *Space Weather*, vol. 10, no. 6, 2012.

[25] "Benchmark Geomagnetic Disturbance Event Description," North American Electric Reliability Corporation (NERC), April 2014.

[26] T. J. Overbye, T. R. Hutchins, K. Shetye, J. Weber, and S. Dahman, "Integration of geomagnetic disturbance modeling into the power flow: A methodology for large-scale system studies," in *2012 North American Power Symposium (NAPS)*. IEEE, 2012, pp. 1–7.

[27] R. Girgis, K. Vedante, and G. Burden, "A process for evaluating the degree of susceptibility of a fleet of power transformers to effects of GIC," in *2014 IEEE PES T&D Conference and Exposition*. IEEE, 2014, pp. 1–5.

[28] P. Picher, L. Bolduc, A. Dutil, and V. Pham, "Study of the acceptable DC current limit in core-form power transformers," *IEEE Transactions on Power Delivery*, vol. 12, no. 1, pp. 257–265, 1997.

[29] M. Lahtinen and J. Elovaara, "GIC occurrences and GIC test for 400 kV system transformer," *IEEE Transactions on Power Delivery*, vol. 17, no. 2, pp. 555–561, 2002.

[30] A. B. Birchfield, T. Xu, K. M. Gegner, K. S. Shetye, and T. J. Overbye, "Grid Structural Characteristics as Validation Criteria for Synthetic Networks," *IEEE Transactions on Power Systems*, vol. 32, no. 4, pp. 3258–3265, 2017.

[31] [Online]. Available: https://electricgrids.engr.tamu.edu/

[32] K. S. Shetye, T. J. Overbye, Q. Qiu, and J. Fleeman, "Geomagnetic disturbance modeling results for the aep system: A case study," in *2013 IEEE Power & Energy Society General Meeting*. IEEE, 2013, pp. 1–5.

[33] D. Boteler, Q. Bui-Van, and J. Lemay, "Directional sensitivity to geomagnetically induced currents of the Hydro-Quebec 735 kV power system," *IEEE Transactions on Power Delivery*, vol. 9, no. 4, pp. 1963–1971, 1994.

[34] R. S. Weigel and D. N. Baker, "Probability distribution invariance of 1-minute auroral-zone geomagnetic field fluctuations," *Geophysical Research Letters*, vol. 30, no. 23, 2003. [Online]. Available: https://agupubs.onlinelibrary.wiley.com/doi/abs/10.1029/2003GL018470